- 1 Inference of photosynthetic capacity parameters from Chlorophyll a
- 2 Fluorescence is affected by redox state of PSII reaction centers
- 3 Jimei Han^{1*}, Lianhong Gu², Jiaming Wen¹, Ying Sun^{1*}
- ⁴ School of Integrative Plant Science, Soil and Crop Science Section, Cornell University, Ithaca,
- 5 NY, USA

9

16

- ²Environmental Sciences Division and Climate Change Science Institute, Oak Ridge National
- 7 Laboratory, Oak Ridge, Tennessee, USA
- *Corresponding to: <u>jh2757@cornell.edu</u> (J. Han), <u>ys776@cornell.edu</u> (Y. Sun)
- 10 This manuscript has been co-authored by UT-Battelle, LLC under Contract No. DE-AC05-00OR22725 with the U.S.
- 11 Department of Energy. The United States Government retains and the publisher, by accepting the article for
- 12 publication, acknowledges that the United States Government retains a non-exclusive, paid-up, irrevocable, worldwide
- 13 license to publish or reproduce the published form of this manuscript, or allow others to do so, for United States
- 14 Government purposes. The Department of Energy will provide public access to these results of federally sponsored
- research in accordance with the DOE Public Access Plan (http://energy.gov/downloads/doe-public-access-plan).

Abstract

18

19

20

21

22

23

24

25

26

27

28

29

30

31

32

33

Solar-Induced chlorophyll Fluorescence (SIF) has been used to infer photosynthetic capacity parameters (e.g., the maximum carboxylation rate $V_{\rm cmax}$, and the maximum electron transport rate J_{max}). However, the precise mechanism and practical utility of such approach under dynamic environments remain unclear. We used the balance between the light and carbon reactions to derive theoretical equations relating chlorophyll a fluorescence (ChlF) emission and photosynthetic capacity parameters, and formulated testable hypotheses regarding the dynamic relationships between the true total ChIF emitted from PSII (SIF_{PSII}) and $V_{\rm cmax}$ and $J_{\rm max}$. We employed concurrent measurements of gas exchanges and ChlF parameters for 15 species from six biomes to test the formulated hypotheses across species, temperatures, and limitation state of carboxylation. Our results revealed that SIF_{PSII} alone is incapable of informing the variations in $V_{\rm cmax}$ and $J_{\rm max}$ across species, even when $SIF_{\rm PSII}$ is determined under the same environmental conditions. In contrast, the product of SIF_{PSII} and the fraction of open PSII reactions q_L , which indicates the redox state of PSII, is a strong predictor of both $V_{\rm cmax}$ and $J_{\rm max}$, although their precise relationships vary somewhat with environmental conditions. Our findings suggest the redox state of PSII strongly influences the relationship between SIF_{PSII} and V_{cmax} and J_{max} .

- 34 **Key words:** Limitation state of carboxylation; photosynthetic capacity; redox state of PSII
- reaction centers; Solar-Induced chlorophyll Fluorescence (SIF)

Introduction

36

37

38

39

40

41

42

43

44

45

46

47

48

49

50

51

52

53

54

55

56

57

58

Photosynthetic capacity, characterized by the maximum carboxylation rate ($V_{\rm cmax}$) of RuBisCO and the maximum electron transport rate (J_{max}) , is prime leaf trait that determine the maximum photosynthetic rate and its response to environmental changes (Wullschleger, 1993; Walker et al., 2014; Wright et al., 2004). V_{cmax} is determined by the amount and kinetics of the active RuBisCO enzyme (ribulose 1,5-bisphosphate carboxylase/oxygenase), the key enzyme for CO₂ fixation during carbon reactions (Cooper, 2000; Yoshikawa, 2013; Detto & Xu, 2020). Under high light conditions, photosynthetic carboxylation is often RuBisCO limited at the current CO₂ level. J_{max} is a key determinant of the potential electron transport rate (J_p) , which becomes the actual electron transport rate (J_a) when photosynthetic carboxylation is limited by the Ribulose 1,5-bisphosphate (RuBP) regeneration (Gu et al., 2019), often under low light conditions at the current CO₂. Timely and accurate estimation of these photosynthetic capacity parameters is of vital importance for reliable prediction of large-scale carbon cycle dynamics and feedbacks to climate change using terrestrial biosphere models (TBMs) (Walker et al., 2014; Rogers et al., 2017) and for field-scale high-throughput crop phenotyping (Meacham-Hensold et al., 2019; Fu et al., 2021). From the perspective of carbon cycle modeling, TBMs (usually coupled with the Intergovernmental Panel on Climate Change IPCC global climate models) have almost exclusively adopted the Farquharvon Caemmerer-Berry (FvCB) biochemical model (Farquhar et al., 1980; von Caemmerer & Farquhar, 1981; von Caemmerer, 2020; Sharkey, 1985), which requires $V_{\rm cmax}$ and $J_{\rm max}$ as key parameters for photosynthesis calculation. Uncertainties in these parameters constitute the major sources of prediction error in the simulated photosynthesis (Bonan et al., 2011; Walker et al., 2014, 2020; Rogers et al., 2017). Their uncertainties come primarily from their huge variability within and across biomes and dependencies on leaf nitrogen/phosphorus, chlorophyll content, age, and

environmental conditions (Field & Mooney, 1986; Xu & Baldocchi, 2013; Monsoon & Baldocchi, 2014; Walker *et al.*, 2014; Croft *et al.*, 2017; Detto & Xu, 2020; Kattge *et al.*, 2020). From the plant breeding perspective towards improving crop yields, increasing the carboxylation capacity of RuBisCO and optimizing electron transport chain are considered as promising genetic modification targets (South *et al.*, 2019; Simkin *et al.*, 2015, 2019; Bailey-Serres *et al.*, 2019). Rapid high-throughput screening of V_{cmax} and J_{max} at the field scale will greatly accelerate the efficiency of selecting crop cultivars with enhanced photosynthesis (Fu *et al.*, 2019, 2021).

59

60

61

62

63

64

65

66

67

68

69

70

71

72

73

74

75

76

77

78

79

80

81

Remote sensing observations, from satellite, airborne, to ground platforms, have been employed to infer these photosynthetic capacity parameters, with spatially and/or temporally resolved details (Croft et al., 2017; Zhang et al., 2014; Serbin et al., 2015; Camino et al., 2019; Meacham-Hensold et al., 2019; Fu et al., 2019, 2021; Yendrek et al., 2017). Such approaches are advantageous over the traditional labor-intensive (though considered as the ground truth) leaf gas exchange measurements (Zhang et al., 2014; Fu et al., 2021). Majority of these remote sensing efforts have been focusing on utilizing multi- or hyper-spectral reflectance from visible, near infrared, to shortwave infrared bands. Recently, Solar-Induced chlorophyll Fluorescence (SIF) emerges as a promising remote sensing tool to infer $V_{\rm cmax}$ and/or $J_{\rm max}$ (Zhang et al., 2014; Camino et al., 2019; Fu et al., 2021). Such promise is driven by the combination of 1) the theoretical grounds established since 1980s that chlorophyll a fluorescence (ChlF) is functionally linked to electron transport for photosynthetic activities at the molecular level (Genty et al., 1989; Papageorgiou & Govindjee, 2004) and 2) the rapidly growing observing capability from satellite, airborne, to ground platforms (Frankenberg et al., 2011; Joiner et al., 2013; Guanter et al., 2012; Mohammed et al., 2019). However, mixed results have been obtained so far with respect to the relationships between SIF (or quantum yield of SIF) and V_{cmax} (or J_{max}). For example, Zhang et al. (2014, 2018) and Camino *et al.* (2019) reported positive SIF- $V_{\rm cmax}$ relationships using ensemble simulations of SCOPE (Soil Canopy Observation Photosynthesis Energy, van der Tol *et al.*, 2009, 2014). In contrast, Vilfan *et al.* (2019) demonstrated that SIF cannot track the variability of $V_{\rm cmax}$ across leaves by combining leaf reflectance and transmittance in SCOPE although the magnitude of $V_{\rm cmax}$ can be estimated with this approach. Fu *et al.* (2021) reported negative relationships between $J_{\rm max}$ (and $V_{\rm cmax}$) and the quantum yield of SIF (Φ_{SIF}) across a variety of tobacco cultivars. Also, Koffi *et al.* (2015) showed weak sensitivity of SIF to $V_{\rm cmax}$ even under high light conditions (usually when carboxylation is RuBisCO limited). These conflicting findings in previous reports have yet to be reconciled.

Conceptually, there is a fundamental mismatch in directly relating $V_{\rm cmax}$ and $J_{\rm max}$ to SIF. The standardized $V_{\rm cmax}$ and $J_{\rm max}$ (i.e., $V_{\rm cmax}25$ and $J_{\rm max}25$ at the reference temperature of 25 °C with no stress) characterize the intrinsic photosynthetic capacity of the carbon and light reactions, respectively. They are supposed to be parameters that do not depend on instantaneous changes in light levels although changes at longer time scales are possible. To the contrary, SIF can only be emitted during the light reactions and vary rapidly with the fluctuating lights in natural environment. Thus, for any SIF - $V_{\rm cmax}$ (or $J_{\rm max}$) relationship to be meaningful, some sort of standardization (i.e., stratification to certain biotic or/and abiotic conditions) must be done for SIF. So far, no studies have examined the best way to standardize SIF for $V_{\rm cmax}/J_{\rm max}$ characterization or how SIF - $V_{\rm cmax}$ (or $J_{\rm max}$) relationships may change under varying light intensities. Further, even with the SIF standardized in one way or the other, it is not immediately clear whether the standardized SIF - $V_{\rm cmax}$ (or $J_{\rm max}$) relationships should be sufficiently invariant to possess at least some predictive power.

This study aims to 1) understand the cause of the discrepancies among existing studies and to 2) develop a mechanistic solution for using SIF observations to infer photosynthetic capacity parameters across species in dynamic environments. We ground our study on the firmly established knowledges of the light and carbon reactions and the balance between the supply and demand of ATP and NADPH. Specifically, we first sought to establish the theoretical basis that links the true total ChIF emitted from PSII (denoted as SIF_{PSII}) and photosynthetic capacity parameters by balancing the actual electron transport rate J_a derived by a mechanistic light reaction model (MLR-SIF, Gu et al., 2019) and that derived by the Farquhar-von Caemmerer-Berry (FvCB) biochemical model (Farquhar et al., 1980). SIF_{PSII} refers to the ChIF prior to signal attenuation due to leaf scattering/reabsorption, which in principle should be utilized to establish the mechanistic relationship with photosynthetic capacity parameters. Our rationale is that the foundation of remotely sensed SIF (i.e., at-sensor SIF) for estimating photosynthetic capacity parameters can only be established once a solid theoretical understanding of fundamental mechanisms that govern the relationships between SIF_{PSII} and photosynthetic capacity parameters is built. We then used the established theoretical basis to formulate testable hypotheses regarding the SIF_{PSII} - $V_{\rm cmax}$ ($J_{\rm max}$) relationships across species in dynamic environments. Finally, we utilized concurrent measurements of leaf-level gas exchanges and ChlF parameters of 15 species from six major plant functional types (PFTs) of the globe to test the theoretically formulated hypotheses. Once these steps were completed, we sought to answer the following questions:

104

105

106

107

108

109

110

111

112

113

114

115

116

117

118

119

120

121

122

123

124

125

- Are there unique, predictive $SIF_{PSII} V_{cmax} / J_{max}$ relationships across species and environmental conditions?
- If not, what factors affect $SIF_{PSII} V_{cmax} / J_{max}$ relationships?
- How can SIF_{PSII} be used to infer V_{cmax} and J_{max} across species in dynamic environments?

Materials and Methods

Theoretical relationships of $V_{\rm cmax}$ and $J_{\rm max}$ with $SIF_{\rm PSII}$ based on the balance between the

light and carbon reactions

Plants have evolved sophisticated mechanisms to ensure that the supply of ATP and NADPH at the end of light reactions balances their demand in the carbon reactions (Rochaix, 2011; Joliot, 2011; Kramer & Evans, 2011). This forms the theoretical basis of our derivation of the mechanistic relationships of V_{cmax} and J_{max} with SIF_{PSII} under varying environmental conditions via the actual electron transport rate J_a . From the perspective of light reactions, we used the mechanistic light reaction model (MLR-SIF) developed by Gu *et al.* (2019) for calculating J_a with SIF_{PSII} together with the fraction of open PSII reactions (q_L) as input (eqn 1).

$$J_a = \frac{\phi_{PSIImax} \cdot (1 + k_{DF})}{1 - \phi_{PSIImax}} \times q_L \times SIF_{PSII}$$
 (eqn 1)

where q_L denotes the fraction of open PSII reactions under the assumption of lake model for photosynthetic unit connectivity, and $\Phi_{PSIImax}$ the maximum photochemical yield of the dark-adapted leaves. $K_{DF} = k_D/k_F$, with k_D and k_F representing the rate constants of constitutive thermal dissipation and fluorescence, respectively. At the present, there are uncertainties regarding the value of k_D and k_F and therefore k_{DF} .

The MLR-SIF model consists of a set of fundamental equations derived from first principles that govern the fate of absorbed photons and relationships among different de-excitation pathways. At their core, these light reaction equations embody the law of conservation of energy in photosystems and are thus universal. Their exact formulation, however, depends on the

connectivity of photosynthetic units, which consist of coupled reaction centers and antenna pigments. Here we used the lake model (Kramer *et al.*, 2004), which assumes that reaction centers are embedded in a network (lake) of antenna pigments such that all photosynthetic units are interconnected and freely share excitations. Such assumption is considered to be highly accurate for higher plants. Detailed derivation of eqn 1 can be found in Gu *et al.* (2019).

147

148

149

150

151

152

153

From the perspective of carbon reactions, we used the classical FvCB model to link J_a with gross photosynthetic rate A_g in C_3 plant species (Farquhar *et al.*, 1980):

154
$$J_a = A_g \times \frac{4C_i + 8\Gamma^*}{C_i - \Gamma^*}$$
 (eqn 2)

Note this equation holds regardless of carboxylation limitation state because J_a is the actual, rather than potential, electron transport rate. A_g (calculated with eqn 3) is essentially the sum of net photosynthetic rate and day respiration. Eqn 2 assumes NADPH supply is limiting. If ATP is limiting, the factor 8 on the right-hand side of eqn 2 should be replaced by the factor 9.33 (Yin *et* al., 2021). Here we did not include TPU-limited carboxylation, as this paper only concerns V_{cmax} and J_{max} .

$$161 A_g = \min \{A_c, A_j\} (eqn 3a)$$

$$A_c = \frac{V_{cmax} \cdot (C_i - \Gamma^*)}{C_i + K_{co}}$$
 (eqn 3b)

163
$$A_j = \frac{J_p}{4} \times \frac{C_i - \Gamma^*}{C_i + 2\Gamma^*}$$
 (eqn 3c)

$$J_p = \frac{\sigma^{\bullet PAR + J_{max} - \sqrt{(\sigma^{\bullet PAR + J_{max}})^2 - 4\theta \cdot \sigma^{\bullet PAR \cdot J_{max}}}}{2\theta}$$
 (eqn 3d)

Here Γ^* and C_i denote the CO₂ compensation point in the absence of mitochondrial respiration and intercellular CO₂ concentration, respectively. K_{co} is a composite parameter for Michaelis-Menten constants for RuBP carboxylation and oxygenation. θ is an empirical curvature parameter and was fixed at 0.9 (Medlyn *et al.*, 2002). σ is the product of $\Phi_{PSIImax}$, leaf light absorptance and fraction of absorbed photons allocated to PSII. σ was set to 0.3 (Long *et al.*, 1993). The values of θ and σ have only a slight effect on the estimated value of J_{max} (Medlyn *et al.*, 2002). J_p is the potential electron transport rate which equals J_a , only under the RuBP regeneration limited carboxylation.

Next, by equating the light reaction-based (MLR-SIF, eqn 1) and carbon reaction-based J_a (FvCB, eqn 2-3), we can derive explicit relationships between SIF_{PSII} and V_{cmax} (and J_{max}) (details in Notes S1). Specifically, under the Rubisco-limited state, we set $A_g = A_c$; then combining eqn 2 and 3b leads to:

$$\frac{V_{cmax} \cdot (C_i - \Gamma^*)}{C_i + Kco} = \frac{(C_i - \Gamma^*)}{4C_i + 8\Gamma^*} \times J_a$$
 (eqn 4)

177 Inserting eqn 1 to eqn 4 results in:

178
$$V_{cmax} = \frac{c_i + \kappa_{co}}{(4c_i + 8\Gamma^*)} \times \frac{\phi_{PSIImax}}{1 - \phi_{PSIImax}} \times (1 + k_{DF}) \times q_L \times SIF_{PSII}.$$
 (eqn 5)

Under the RuBP regeneration limited state, the potential electron transport rate becomes the actual rate, *i.e.*, $J_p = J_a$, then equating eqn 1 and eqn 3d leads to

$$I81 \quad J_{max} = \frac{\theta \cdot \frac{q_L \cdot SIF_{PSII} \cdot (1+k_{DF})}{\sigma \cdot PAR} - \frac{1-\Phi_{PSIImax}}{\Phi_{PSIImax}}}{\frac{q_L \cdot SIF_{PSII} \cdot (1+k_{DF})}{\sigma \cdot PAR} - \frac{1-\Phi_{PSIImax}}{\Phi_{PSIImax}}} \times \frac{\Phi_{PSIImax}}{1-\Phi_{PSIImax}} \times (1+k_{DF}) \times q_L \times SIF_{PSII}$$
 (eqn 6)

To obtain $V_{\text{cmax}25}$ and $J_{\text{max}25}$, *i.e.*, V_{cmax} and J_{max} values at the 25 °C reference temperature, we invoked the temperature response function $f_v(T)$ and $f_i(T)$ respectively (eqn 7a, 7b). We adopted

Arrhenius function (Arrhenius, 1915) for $f_v(T)$ and the peaked function (Johnson *et al.*, 1942) for $f_v(T)$ according to Medlyn *et al.* (2002).

$$V_{cmax} = V_{cmax25} f_V(T)$$
 (eqn 7a)

187
$$J_{max} = J_{max25} f_J(T)$$
 (eqn 7b)

- where T represents the leaf temperature.
- 189 This leads to:

190
$$V_{cmax25} = \frac{1}{f_V(T)} \times \frac{C_i + Kco}{(4C_i + 8\Gamma^*)} \times \frac{\Phi_{PSIImax}}{1 - \Phi_{PSIImax}} \times (1 + k_{DF}) \times q_L \times SIF_{PSII}$$
 Rubisco-limited (eqn 8)

191
$$J_{max25} = \frac{1}{f_J(T)} \times \frac{\theta \cdot \frac{q_L \cdot SIF_{PSII} \cdot (1+k_{DF})}{\sigma \cdot PAR} - \frac{1-\Phi_{PSIImax}}{\Phi_{PSIImax}}}{\left(\frac{q_L \cdot SIF_{PSII} \cdot (1+k_{DF})}{\sigma \cdot PAR} - \frac{1-\Phi_{PSIImax}}{\Phi_{PSIImax}}\right)} \times \frac{\Phi_{PSIImax}}{1-\Phi_{PSIImax}} \times (1+k_{DF}) \times q_L \times SIF_{PSII}$$

RuBP regeneration-limited (eqn 9)

Eqn 5-6 and 8-9 lay the foundation for interpreting and modeling the dynamic relationship between SIF_{PSII} and photosynthetic capacity parameters under changing environmental conditions. Note that under Rubisco-limited state, only the functional relationship of V_{cmax} with SIF_{PSII} was derived; but a similar relationship is expected for J_{max} with SIF_{PSII} , as it has been well established that V_{cmax} and J_{max} are highly correlated across a broad range of plant biomes (Wullschleger, 1993; Walker et al., 2014). The same argument holds true for V_{cmax} and J_{max} under the RuBP regeneration limited state. Also, we did not consider the TPU-limited carboxylation state here, as this study focuses on V_{cmax} and J_{max} only; but the relationship between TPU and SIF_{PSII} can be similarly derived following the same procedure above.

From eqn 5 (and 8), it is immediately clear that, under Rubisco-limitation state, the relationship of SIF_{PSII} with V_{cmax} (and by extension with J_{max}) depends on environmental conditions, because q_L , C_i , K_{co} , and Γ^* all vary with environmental conditions (*i.e.*, PAR and/or temperature). Under RuBP regeneration limitation stage in eqn 6 (and 9), the relationship of SIF_{PSII} with J_{max} (and also by extension with V_{cmax}) depends on q_L and PAR, which are highly dynamic with environmental changes. Therefore, we hypothesize the following:

- **Hypothesis I**: There is no unique relationship between $V_{\text{cmax}25}$ (and $J_{\text{max}25}$) and SIF_{PSII} .
- **Hypothesis II**: $V_{\text{cmax}25}$ and $J_{\text{max}25}$ are positively correlated with the product of q_{L} and SIF_{PSII} , *i.e.*, $SIF_{\text{PSII}} \times q_{\text{L}}$ (measured at the same environmental conditions).
- When Rubisco limits carboxylation (eqn 8), $\frac{1}{f_V(T)} \times \frac{C_i + Kco}{(4C_i + 8\Gamma^*)}$ should regulate the strength of the relationship between $V_{\text{cmax}25}$ ($J_{\text{max}25}$) and $SIF_{\text{PSII}} \times q_{\text{L}}$. As remote sensing SIF-based $V_{\text{cmax}}/J_{\text{max}}$ inference applies only to the ambient CO₂ (C_a), the variation in $\frac{C_i + Kco}{4C_i + 8\Gamma^*}$ should be mainly due to variations in temperature if the C_i/C_a ratio is assumed to be constant. The relationship of $V_{\text{cmax}25}$ and $J_{\text{max}25}$ with $SIF_{\text{PSII}} \times q_{\text{L}}$ will be affected by the joint temperature dependence of $\frac{C_i + Kco}{4C_i + 8\Gamma^*}$ and $f_V(T)$. This motivates the third hypothesis:
- **Hypothesis III**: Under the Rubisco limitation, temperature variations increase the variability of the relationship of $V_{\text{cmax}25}$ and $J_{\text{max}25}$ with $SIF_{\text{PSII}} \times q_{\text{L}}$.
- When RuBP regeneration limits carboxylation, eqn 9 reveals that $V_{\rm cmax}$ or $J_{\rm max}$ is not simply
- 220 linearly related to $SIF_{PSII} \times q_L$. The term $(\frac{SIF_{PSII}}{\sigma \bullet PAR})$ in the slope $(\frac{\theta \bullet \frac{q_L \bullet SIF_{PSII} \bullet (1+k_{DF})}{\sigma \bullet PAR} \frac{1-\Phi_{PSIImax}}{\Phi_{PSIImax}}}{(\frac{q_L \bullet SIF_{PSII} \bullet (1+k_{DF})}{\sigma \bullet PAR} \frac{1-\Phi_{PSIImax}}{\Phi_{PSIImax}}})$

approximately equals to Φ_{SIF} and has been shown to be relatively muted to PAR variations (Gu *et al.*, 2019), but q_L is very sensitive to instantaneous variations in the environment factors (*e.g.*, PAR, water stress, besides temperature). This reasoning leads to the fourth hypothesis:

- **Hypothesis IV**: $V_{\text{cmax}25}$ and $J_{\text{max}25}$ have stronger linear relationships with $SIF_{\text{PSII}} \times q_{\text{L}}$ under Rubisco-limited than under RuBP regeneration-limited carboxylation state.

Testing these hypotheses with the concurrent measurements of leaf-level gas exchanges and ChlF parameters at the leaf level is essential to better understanding how *SIF*_{PSII} should be used to infer photosynthetic capacity parameters.

Study sites and plant species

230

231

232

233

234

235

236

237

238

239

240

241

242

243

244

245

246

247

248

249

250

251

252

To test the hypotheses inferred from theory above, we used measurements conducted at the Oak Ridge National Laboratory (ORNL), Oak Ridge, TN, U.S. (35°54'N; 84°20'W) from July to October in 2017, and Cornell Botanic Gardens (CBG), Ithaca, NY, U.S. (42°26'N; 76°28'W) from June to August in 2020. We collected concurrent measurements of leaf gas exchanges and ChlF parameters for 15 plant species (Table 1) from six major PFTs. At CBG, the average annual maximum and minimum temperatures are 13.61 °C and 2.64 °C, respectively and the average annual precipitation is 789 mm. The measured species cover boreal broadleaf deciduous trees (BDT Boreal), temperate broadleaf deciduous shrubs (BDS Temperate), temperate broadleaf deciduous trees (BDT Temperate), and C₃ Grass (C3G). Measurements at ORNL were made for two-vear-old bare-root tree saplings and cotton grown in walk-in growth chambers. The tree saplings were from species that are representative of temperate broadleaf deciduous trees (BDT-Temperate) and boreal needle evergreen trees (NET-Boreal). They were planted into 6.2 L plastic pots filled with standard potting mix (Sungro, Canada), and maintained under natural sunlight, air temperature and humidity. Ten months later, healthy uniform plants were transplanted into 35 L pots with the same soil mix and grown for 30 days in a walk-in growth chamber (expanded temperature range Model BDW80, Conviron, Canada) before measurements were collected in July, 2017. The maximum PAR in the walk-in growth chamber was set to 1200 umol m⁻² s⁻¹. We planted two cotton species for this study. Cotton seeds were planted in 10 L pots using the standard potting mix on October 6, 2017 in a greenhouse. Supplemental lighting was turned on for 14h per day using HPS 1000 W growth lights that maintained light inside the greenhouse above ~400 µmol m⁻¹ ² s⁻¹. Greenhouse air temperatures were set to 28 °C for the 14 h photoperiod and 25 °C at night. After 60 days, the plants were moved to the growth chamber for targeted measurements under

carefully controlled diurnal environmental conditions. After 14 days of acclimation, the topmost fully expanded leaves on the main stem were selected for experiments. All species at ORNL were irrigated and fertilized periodically with 20-10-20 NPK fertilizer (Southern AG, USA).

Table 1. Description of plant species, the corresponding Plant Functional Types (PFTs), growth stage, and location.

Plant Functional Types (PFTs)	Species	Plant growth stage	Measured temperature (°C)	Location
Broadleaf deciduous tree-boreal	Betula alleghaniensis (BA)	Mature plant	25	CBG
(BDT Boreal)	Betula papyrifera (BP)	Mature plant	25	CBG
C ₃ Grass	Dichanthelium clandestinum (DC)	Mature plant	25	CBG
Broadleaf deciduous shrub-temperate (BDS Temperate)	Cornus racemosa 'Cuyzam' (CRC)	Mature plant	25	CBG
	Viburnum dentatum 'Christom' (VD)	Mature plant	25	CBG
	Cornus racemosa 'Ottzam' (CRO)	Mature plant	25	CBG
Broadleaf deciduous tree-temperate	Juglans nigra (JN)	Mature plant	25	CBG
	Carya ovata 'Wilcox' (CAO)	Mature plant	25	CBG
(BDT Temperate)	Liquidambar styraciflua 'Moraine' (LSM)	Mature plant	25	CBG

	Quercus shumardii Buckl.	Seedlings	20, 25, 30, 35, 40,	ORNL
	(QUSH)		45	
	Quercus falcata Michx. (QUFA)	Seedlings	20, 25, 30, 35, 40, 45	ORNL
	Liriodendron tulipifera L. (LITU)	Seedlings	20, 25, 30, 35, 40,	ORNL
			45	
Needleleaf evergreen				_
tree-Boreal	Pinus strobus L. (PIST)	Seedlings	25	ORNL
(NET Boreal)				
C ₃ Crops	Gossypium hirsutum L. (GH)	Flowering Stage	25	ORNL
	Gossypium barbadense L. (GB)	Flowering Stage	25	ORNL

Measurement protocols of leaf gas exchanges and ChIF parameters

We measured both light and CO₂ response curves of gas exchanges and ChlF for each species at CBG and ORNL. For each curve, we selected three to five healthy and fully expanded leaves as replicates of each species. At CBG, curves were measured with GFS-3000 (Walz, Effeltrich, Germany) equipped with fluorescence measuring head (3010-S, Walz). At ORNL, these curves were measured with LI-6800 (LI-COR Inc., Lincoln, NE, USA) equipped with leaf multiphase flash fluorometer chamber (6800-01A, LI-COR Inc). For GFS-3000, RH was kept between 50% and 60%, the flow rate at 700 mL min⁻¹, and the leaf temperature at 25 °C. Prior to actual measurements of light and CO₂ response curves, photosynthesis was first induced with a saturating light intensity. Once the steady state was reached (usually within 20 minutes), the auto-progress

of light and CO₂ response curve was adopted. We performed light response curve measurements following a sequence of PAR intensities: 2000, 1800, 1500, 1200, 1000, 800, 500, 300, 200, 150, 100, 50, 0 μmol photon m⁻² s⁻¹ respectively, with CO₂ concentration in the leaf chamber provided by a CO₂ cylinder maintained constant at 400 μmol mol⁻¹. Following the light response curve measurements, we collected CO₂ response curves on the same leaves following a sequence of CO₂ concentrations: 400, 300, 200, 150, 100, 50, 0, 380, 550, 800, 1000, 1200, 1500 μmol CO₂ mol⁻¹ under the saturated light intensity (2000 μmol m⁻² s⁻¹ for species at CBG; 1200 and 1500 μmol m⁻² s⁻¹ for species at ORNL). These light and CO₂ response curves were measured at 25°C, the reference temperature commonly used for standardizing photosynthetic parameters. Furthermore, for each individual leaf within a subset of plant species (LITU, QUSH, and QUFA) grown in the walk-in growth chamber at ORNL, we collected additional light and CO₂ response curves of gas exchanges and ChlF parameters under different leaf temperatures, 20, 25, 30, 35, 40, and 45 °C, respectively, with the same protocols described above.

After collecting the light and CO₂ response curves, which can be used to obtain gas exchange variables (*i.e.*, the intercellular CO₂ concentration - C_i) and steady-state and maximum ChlF under light conditions (F_s and F_m '), we subsequently measured the maximum and minimum ChlF under fully dark-adapted conditions (F_m and F_o) for each leaf replicate under 25 °C. To achieve this, we first marked the measured area of each dark-adapted leaf to keep the same measuring position as during the response curve measurements. We wrapped the measured leaf with aluminum foil, dark-adapted it for at least half an hour, and then recorded F_o and F_m . The responses of F_m and F_o on temperatures (Pospisil *et al.*, 1998) were used to obtain the values of F_m and F_o at other temperatures (20, 30, 35, 40, and 45 °C) in LITU, QUSH, and QUFA.

Derivation of ChlF related variables

- The measured ChlF parameters were in turn used to calculate the following ChlF related variables,
- including minimum ChlF under light (F_0) , q_L , non-photochemical quenching (NPQ), SIF_{PSII} and
- the actual electron transport rate (J_a). Specifically:

295
$$F_o' = \frac{F_o}{\Phi_{PSIImax} + \frac{F_o}{Fm'}}$$
 (Oxborough & Baker, 1997) (eqn 10)

- where $\Phi_{PSIImax}$ denotes the maximum photochemical yield in the dark-adapted leaves calculated as
- 297 $(F_{\rm m}-F_{\rm o})/F_{\rm m}$.

298
$$q_{\rm L} = \frac{F'_m - F_s}{F'_m - F'_o} \times \frac{F'_o}{F_s}$$
 (Kramer *et al.*, 2004) (eqn 11)

299 NPQ=
$$\frac{F_m - F'_m}{F'_m}$$
 (Genty *et al.*, 1989) (eqn 12)

- Then the leaf-level SIF_{PSII} was computed from the following theoretical equations (Porcar-
- 301 Castell *et al.*, 2014; Gu *et al.*, 2019):

302
$$SIF_{PSII} = \Phi_{SIF} \times PAR \times \alpha \times \beta$$
 (eqn 13)

303
$$\Phi_{SIF} = \frac{1 - \Phi_{PSIImax}}{(1 + k_{DF}) \times [(1 + NPQ) \times (1 - \Phi_{PSIImax}) + q_L \times \Phi_{PSIImax}]}$$
 (eqn 14)

- where α is leaf absorptance and assumed to be 0.84 (Björkman & Demmig, 1987, Schreiber, 2004);
- β the fraction of light allocated to PSII, assumed to be 0.5 (von Caemmerer, 2000). It is assumed
- here that $k_{\rm DF}$ is 10 according to the suggestion of Pfündel (1998) rather than 19 adopted by Gu et
- 307 al. (2019). The rationale is that the magnitude and range of $\Phi_{\rm SIF}$ calculated with a $k_{\rm DF}$ value of 10
- 308 (eqn 14) could match the absolute fluorescence yield directly measured by Tesa et al. (2018).

Further, J_a was calculated with eqn 1 from SIF_{PSII} and q_L or directly from PAM parameters (Genty *et al.*, 1989; Schreiber, 2004; Gu et al., 2019):

312
$$J_a = \frac{F'_m - F_s}{F'_m} \times PAR \times \alpha \times \beta$$
 (eqn 15)

The J_a formulations for eqn 1 and eqn 15 are theoretically identical although they use different parameters as inputs (Gu *et al.*, 2019).

Estimation of $V_{\rm cmax}$ and $J_{\rm max}$

315

316

317

318

319

320

321

322

323

324

325

326

327

328

329

330

We did not employ the theoretical formulations (eqn 5-6 and eqn 8-9) to directly calculate $V_{\rm cmax}$ and J_{max} in this study, as the actual values of the input parameters (e.g., Γ^* , Kco, k_{DF} , θ , and σ) are currently unknown although they have been considered as constants (note the validity of these equations were still validated in Note S2). Instead, to estimate $V_{\rm cmax}$ and $J_{\rm max}$, we adopted the traditional approach, i.e., fitting CO₂ response curves based upon the FvCB model (Farquhar et al., 1980; Sharkey, 1985) using the *photosynthesis* R package (Stinziano *et al.*, 2020). This approach adopts the fitting strategy of Gu et al. (2010), which iterates all possible C_i transitional points in order to automate the determination of the carboxylation limitation state, removal of inadmissible curves fits, and selection of the best fit by minimizing the cost function. Default parameters (i.e., Γ^* , K_c , and K_o) and temperature response function were all from Bernacchi et al. (2001). Mesophyll conductance was assumed to be infinite for the present study (its limitation discussed in Notes S2). By default, this *photosynthesis* R package does not output the actual carboxylation limitation state, we thus conducted forward simulations of FvCB with the fitted parameter along with PAR and CO₂ concentration, and used the resulting minimal carboxylation rate as the output actual limiting state. We repeated this procedure for each leaf replicate under their measured

- temperatures. To better distinguish from V_{cmax25} and J_{max25} , V_{cmax} and J_{max} at measuring leaf
- temperatures in the following content were denoted by $V_{\rm cmax-T}$ and $J_{\rm max-T}$, respectively.

Results

333

334

335

336

337

338

339

340

341

342

343

344

345

346

347

348

349

350

351

352

353

354

Relationships of photosynthetic capacity parameters with SIF_{PSII}, q_L, and SIF_{PSII}×q_L

(Hypotheses I and II)

We first evaluated the relationships between photosynthetic capacity parameters ($V_{\rm cmax25}$ and $J_{\rm max25}$) and SIF_{PSII} derived from ChlF measurements across 15 different plant species (grouped into six PFTs) under the light intensity of 1200 µmol m⁻² s⁻¹, ambient CO₂ concentration, and 25 °C. We did not observe any detectable relationships between SIF_{PSII} and J_{max25} (R²=0.01, Fig. 1a) or V_{cmax25} $(R^2=0.07, Fig. 1d)$. This suggests that SIF_{PSII} itself alone is unable to capture the variation of V_{cmax25} and $J_{\text{max}25}$ across plant species, even under strictly controlled environmental conditions. In contrast, once q_L variation is accounted for, we found striking relationships between $SIF_{PSII} \times q_L$ and both photosynthetic capacity parameters, i.e., $R^2 = 0.76$ (p < 0.05) for $J_{\text{max}25}$ and $R^2 = 0.64$ (p<0.05) for $V_{\text{cmax}25}$ respectively (Fig. 1b,e). q_L itself is also significantly related to $J_{\text{max}25}$ (R²=0.67, p<0.05, Fig. 1c) and $V_{\text{cmax}25}$ (R²=0.45, p<0.05, Fig. 1f) across plant species. However, compared to $SIF_{PSII} \times q_L$, the explanatory power of q_L for $J_{\text{max}25}$ and V_{cmax} is reduced by 12% and 30%, respectively. These patterns suggest that $SIF_{PSII} \times q_L$ is a much more effective predictor to infer photosynthetic capacity parameters than SIF_{PSII} or q_L itself alone. This is because $SIF_{PSII} \times q_L$ not only contains the information of fluorescence emissions, but also, implicitly, that of NPQ dynamics which regulates the relationships of SIF_{PSII} with photosynthetic capacity, according to the principle of energy balance (i.e., eqn 20 in Gu et al., 2019, more details in Discussions). Our results directly drawn from measurements confirm our Hypothesis I and II formulated from theoretical reasoning. Still the $SIF_{PSII} \times q_L - V_{cmax}/J_{max}$ relationships can to some degree vary across PFTs (Fig. 1), likely a consequence of other parameters that were assumed to be constant but can differ among plant

species (e.g., Γ^* and Kco in eqn 5, detailed discussions in Notes S2) and the specific growth conditions in natural environments (e.g., varying climates, soil conditions, topography, among others, detailed discussion below).

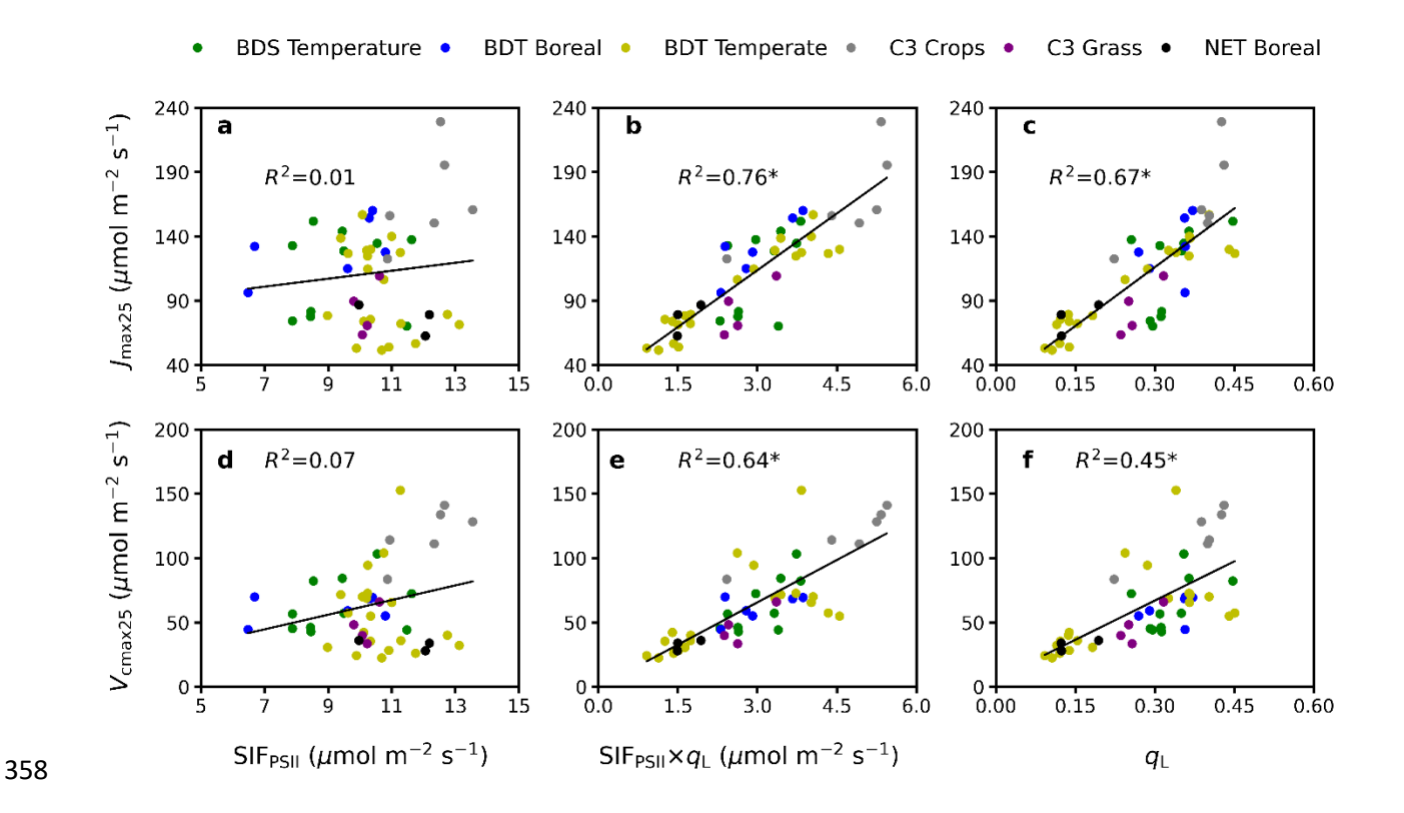


Fig. 1. The relationships of SIF_{PSII} with J_{max25} (a) and V_{cmax25} (d), the relationships of $SIF_{PSII} \times q_L$ with J_{max25} (b) and V_{cmax25} (e), and the relationships of q_L with J_{max25} (c) and V_{cmax25} (f) respectively, across 15 plant species grouped into six plant function types (PFTs, Table 1). Here, SIF_{PSII} was calculated with the ChIF parameters (eqn 13) at PAR of 1200 μ mol m⁻² s⁻¹, ambient CO₂ concentration (400 μ mol mol⁻¹), and 25 °C. J_{max25} and J_{cmax25} were fitted with the FvCB model at 25 °C. Each scatter represents one leaf replicate, color coded by PFTs. The black lines are linear ordinary least-square regression with all leaves pooling together. * denotes a statistically significant at the significance level of 0.05.

Impact of temperature variations on the relationships of photosynthetic capacity parameters with SIF_{PSII} , q_L , and $SIF_{PSII} \times q_L$ (*Hypothesis III*)

368

369

370

371

372

373

374

375

376

377

378

379

380

381

382

383

384

For a subset of plant species, light and CO₂ response curves were collected under varying temperatures ranging from 20 °C to 45 °C (Table 1). For these species, we found that under the Rubisco-limited state, $J_{\text{max-T}}$ ($V_{\text{cmax-T}}$) can be either positively or negatively correlated with SIF_{PSII} (under the same temperature) as temperature varies, and none of their relationships are statistically significant except for the correlation at 30 °C (Fig. 2a,d). In contrast, there are strong correlations of $SIF_{PSII} \times q_L$ with J_{max-T} (R²=0.71) and with V_{cmax-T} (R²=0.80) when all plant species are pooled together (Fig. 2b,e). Also, q_L is significantly related to $J_{\text{max-T}}$ and $V_{\text{cmax-T}}$, with 66% and 65% of the variability of $J_{\text{max-T}}$ (Fig. 2c) and $V_{\text{cmax-T}}$ (Fig. 2f) being explained by q_{L} . The relationships between $SIF_{PSII} \times q_L$ and J_{max-T} (V_{cmax-T}) are stronger than that between q_L and J_{max-T} (V_{cmax-T}) at a single temperature or across all the temperatures. This indicates that SIF_{PSII} alone, to a certain extent, can constraint (not accurately estimate though) the variability of photosynthetic capacity parameters across plant species. $SIF_{PSII} \times q_L$ can infer photosynthetic capacity parameters more accurately than SIF_{PSII} or q_L itself alone across temperatures. Interestingly, the regression slopes of $SIF_{PSII} \times q_L$ (Fig. 2b,e) against J_{max-T} (V_{cmax-T}) are relatively stable across a broad range of temperature variation under Rubisco limitation.

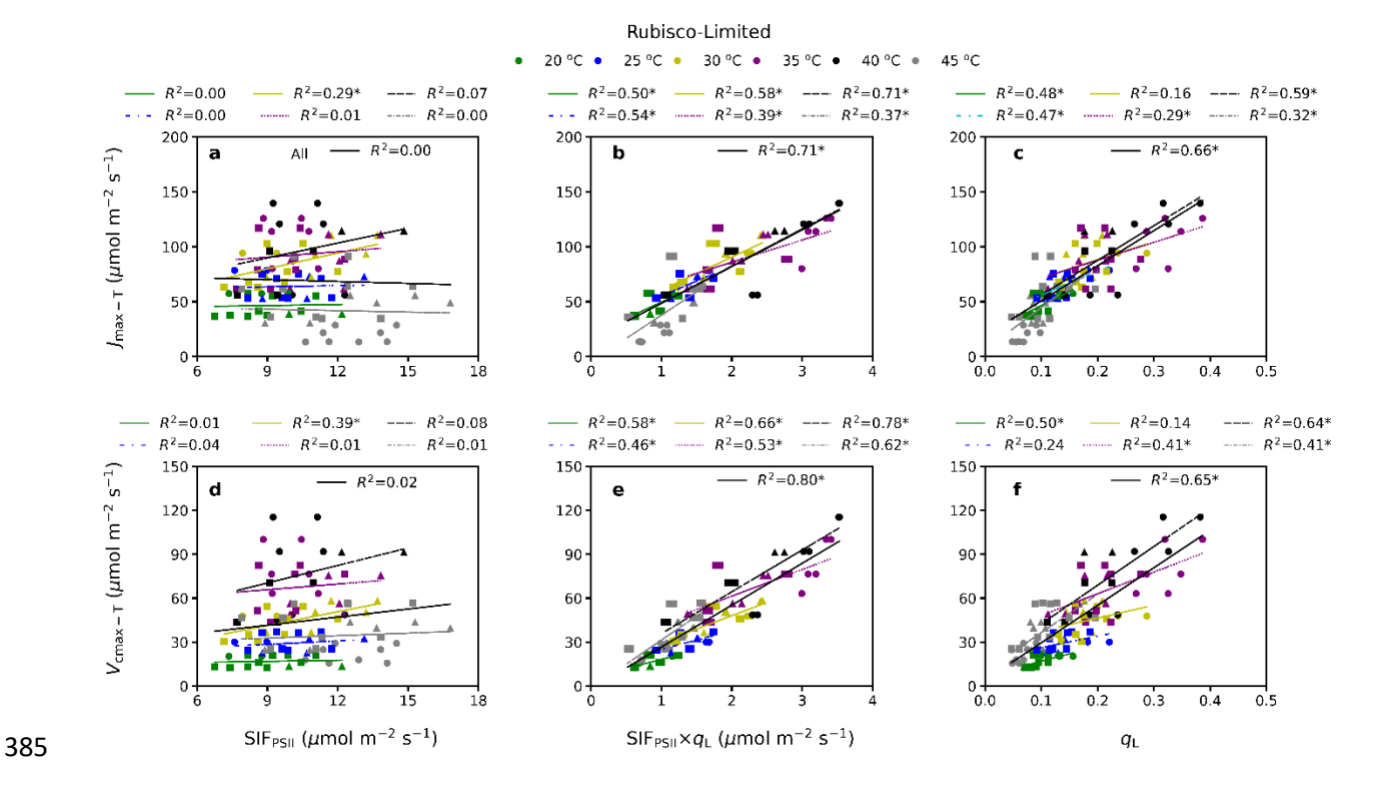


Fig. 2. Impact of temperature variations on the relationship of $J_{\text{max-T}}$ (and $V_{\text{cmax-T}}$) with SIF_{PSII} (a, d), $SIF_{\text{PSII}} \times q_{\text{L}}$ (b, e), and q_{L} (c, f). Similar to Fig.1, but the relationships were analyzed under Rubisco-limited state for a subset of plant species that were measured under different temperatures, *i.e.* 20 °C (n = 14), 25 °C (n = 16), 30 °C (n = 16), 35 °C (n = 20), 40 °C (n = 12), 45 °C (n = 24). SIF_{PSII} and $SIF_{\text{PSII}} \times q_{\text{L}}$ were calculated with eqn 13 under the PAR of 1200 and 1000 μmol m⁻² s⁻¹. The data size (n) depends on how many data samples were Rubisco-limited under each temperature. $J_{\text{max-T}}$ and $V_{\text{cmax-T}}$ were fitted with the FvCB model at these individual temperatures. Each scatter represents one single leaf, separated by plant species (circle: LITU, triangle: QUSH, square: QUFA), and grouped by temperature.

When normalizing $J_{\text{max-T}}$ (and $V_{\text{cmax-T}}$) to the reference temperature 25 °C, their strong correlation with $SIF_{\text{PSII}} \times q_{\text{L}}$ remains relatively stable but their regression slopes diverge considerably (Fig. 3b,e). This pattern suggests that, under the Rubisco limitation, temperature

variations can further complicate the relationships of $V_{\text{cmax}25}$ and $J_{\text{max}25}$ with $SIF_{\text{PSII}} \times q_{\text{L}}$, confirming 398 our Hypothesis III. Such divergence of regression slopes is likely a consequence of the regulation 399 of $f_V(T)$ and $f_J(T)$. This is supported by Fig. 4, which shows the composite terms $(\frac{C_i + Kco}{(4C_i + 8\Gamma^*)})$ and 400 $(\frac{\theta \bullet \frac{q_L \bullet SIF_{PSII} \bullet (1+k_{DF})}{\sigma \bullet PAR} - \frac{1 - \Phi_{PSIImax}}{\Phi_{PSIImax}}}{\frac{q_L \bullet SIF_{PSII} \bullet (1+k_{DF})}{\sigma \bullet PAR} - \frac{1 - \Phi_{PSIImax}}{\Phi_{PSIImax}}}) \text{ in eqn 8 and 9 respectively are relatively stable across different}$ 401 temperatures (Fig. 4c,d), compared to if when $f_V(T)$ and $f_I(T)$ are included (Fig. 4a,b). This 402 analysis mimics the actual applications of remote sensing SIF (measured under dynamic 403 temperatures) for inferring $V_{\text{cmax}25}$ and $J_{\text{max}25}$. In addition, a weaker relationship of $J_{\text{max}25}$ (and 404 405 V_{cmax25}) with q_{L} than with $SIF_{\text{PSII}} \times q_{\text{L}}$ was observed under each temperature (Fig. 3b, e versus Fig. 3c, f). However, when all the data at different temperatures were pooled together, the explanatory 406 power of $SIF_{PSII} \times q_L$ for J_{max25} and V_{cmax25} is similar to or even lower than that of q_L alone. This 407 indicates that SIF_{PSII} cannot capture the variability of J_{max25} and V_{cmax25} caused by temperatures 408 (also confirm by Fig. 5d below). Note the dependence of k_D on the temperature (van der Tol et al., 409 2014) may affect the response of SIF_{PSII} on temperatures, but k_D and k_F are fundamental physical 410 properties of the chlorophyll molecule and there is current no physical mechanism to explain the 411

dependence of k_D (an antenna process) on temperature.

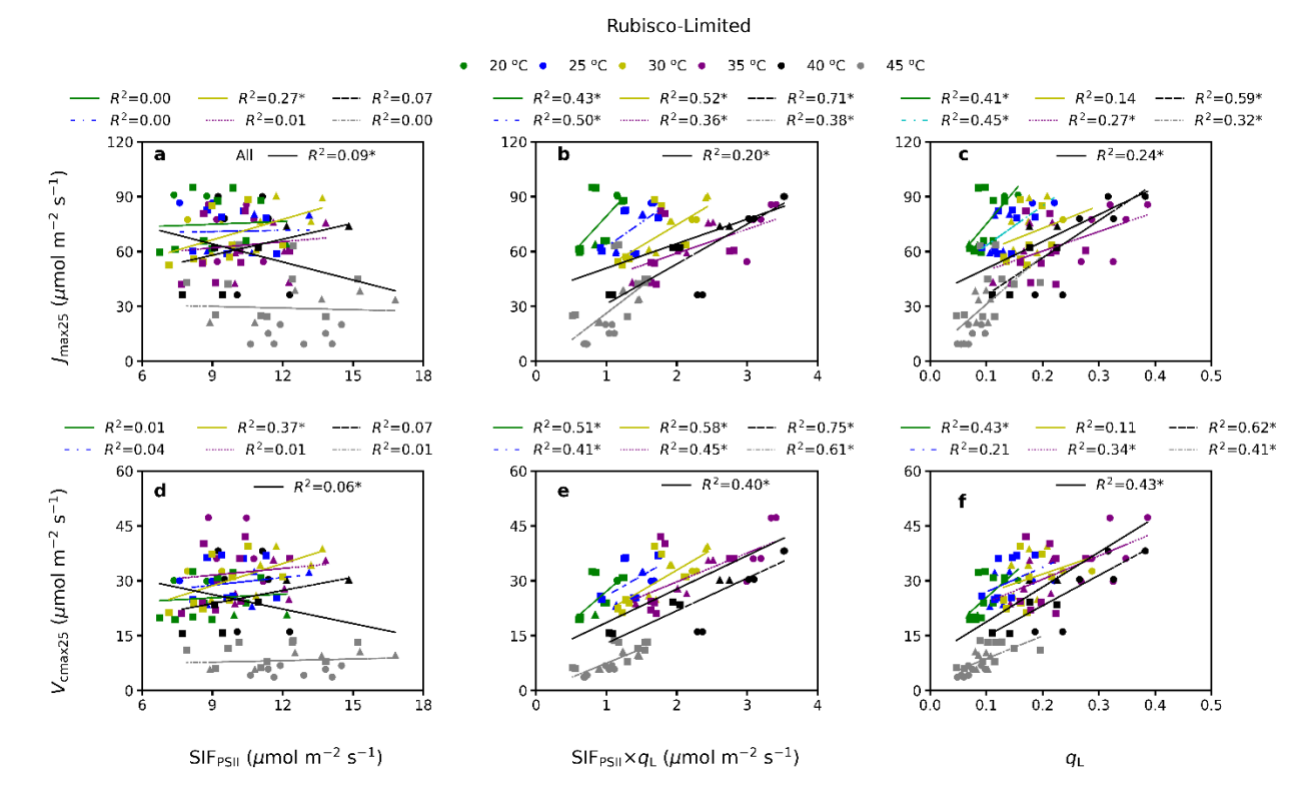


Fig. 3. Similar to Fig.2 except $V_{\text{cmax-T}}$ and $J_{\text{max-T}}$ were normalized to 25 °C, *i.e.*, for V_{cmax25} and J_{max25} .

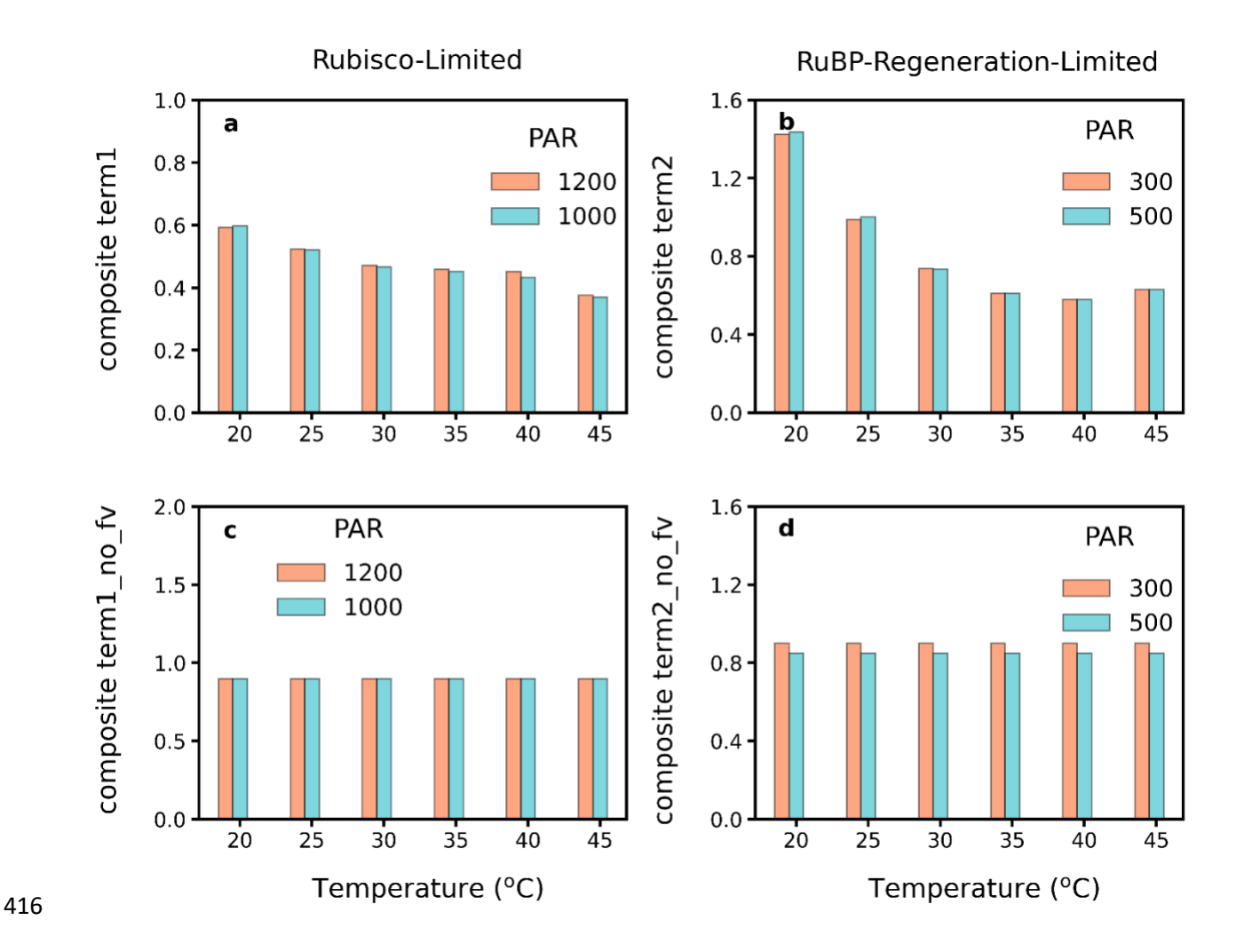


Fig. 4. The variations of the composite term of eqn 8 $(\frac{1}{f_V(T)} \times \frac{C_i + Kco}{4C_i + 8\Gamma^*}, a; \frac{C_i + Kco}{4C_i + 8\Gamma^*}, c)$ and of eqn 9

418
$$(\frac{1}{f_V(T)} \times \frac{\theta \bullet \frac{q_L \bullet SIF_{PSII} \bullet (1+k_{DF})}{\sigma \bullet PAR} - \frac{1-\Phi_{PSIImax}}{\Phi_{PSIImax}}}{\frac{q_L \bullet SIF_{PSII} \bullet (1+k_{DF})}{\sigma \bullet PAR} - \frac{1-\Phi_{PSIImax}}{\Phi_{PSIImax}}}, b; \frac{\theta \bullet \frac{q_L \bullet SIF_{PSII} \bullet (1+k_{DF})}{\sigma \bullet PAR} - \frac{1-\Phi_{PSIImax}}{\Phi_{PSIImax}}}{\frac{q_L \bullet SIF_{PSII} \bullet (1+k_{DF})}{\sigma \bullet PAR} - \frac{1-\Phi_{PSIImax}}{\Phi_{PSIImax}}}, d) \text{ with } (a,b) \text{ and without }$$

(b,d) the consideration of temperature function under different temperatures. Different colors represent different PAR. Each bar represents the mean of all the replicate individuals in three species (LITU, QUSH, and QUFA).

To understand why the $SIF_{PSII} \times q_L \sim V_{cmax-T}$ (J_{max-T}) relationships can hold relatively stable across temperatures under the Rubisco limitation, we compared the temperature dependence of

SIF_{PSII} with those of q_L , and V_{cmax-T} (J_{max-T}) (Fig. 5). We found that temperatures have stronger impact on q_L and V_{cmax-T} (J_{max-T}) than on SIF_{PSII}. For example, for all species, q_L and V_{cmax-T} (J_{max-T}) increase almost in parallel as a function of temperature from 20°C to 35°C and then both declined at higher temperatures (Fig. 5a,b,c). Such consistency in the variations of q_L and V_{cmax-T} (J_{max-T}) with temperatures implies that q_L can reflect the activation of the carboxylation enzyme. In contrast, SIF_{PSII} does not exhibit much variation with temperature (Fig. 5d), likely a consequence of the dominant role of light on SIF_{PSII}. Collectively, the product of SIF_{PSII} and q_L can effectively characterize the temperature impacts on V_{cmax-T} (J_{max-T}) (Fig. 5e).

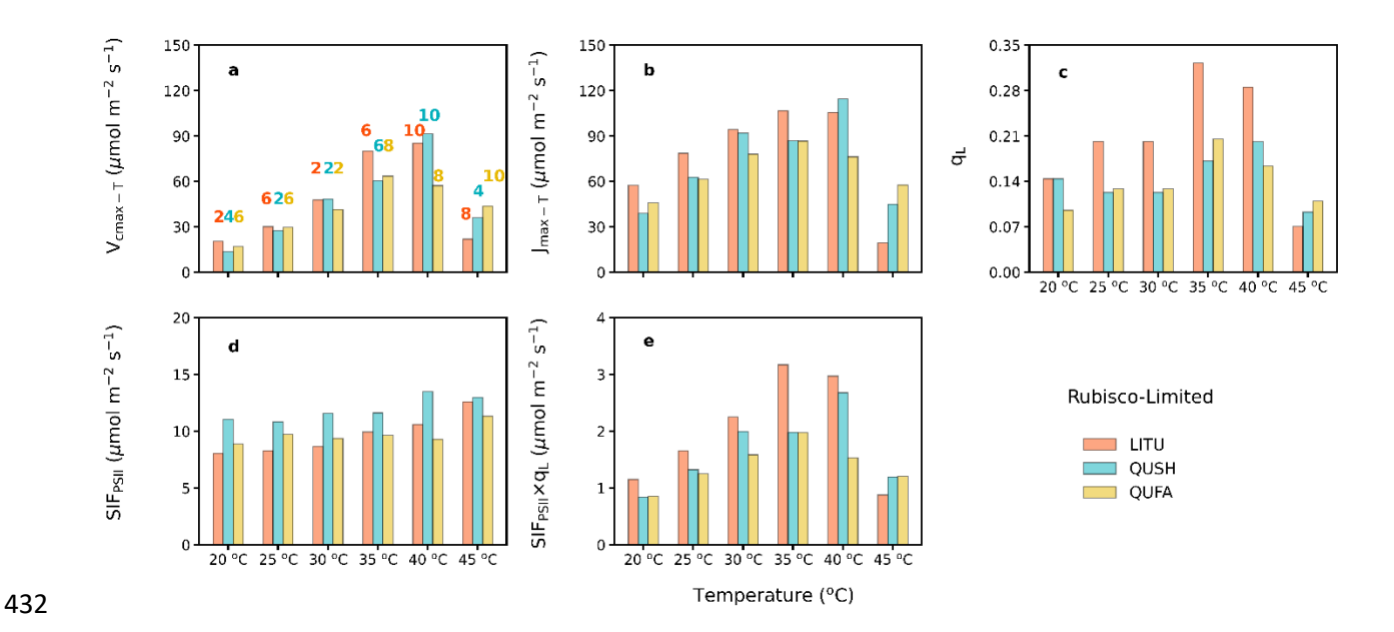


Fig. 5. The variations of $V_{\text{cmax-T}}$ (a), $J_{\text{max-T}}$ (b), q_{L} (c), SIF_{PSII} (d), and $SIF_{\text{PSII}} \times q_{\text{L}}$ (e) under different temperatures for three species (LITU, QUSH, QUFA). Each bar represents the mean of leaf replicates within the same temperature under the Rubisco limited state, the number of replicates is shown above each bar.

Carboxylation limitation states must be considered for using SIF_{PSII} to infer photosynthetic capacity parameters (Hypothesis IV)

As SIF_{PSII} (and also q_L) varies instantaneously with PAR while photosynthetic capacity parameters have no dependence on PAR, we further examined whether and how carboxylation limitation state (which depends on PAR) alters the relationship between SIF_{PSII} (and $SIF_{PSII} \times q_L$) and J_{max25} (and V_{cmax25}). We found that $SIF_{PSII} \times q_L$ is more tightly related to J_{max25} (and V_{cmax25}) linearly under Rubisco-limited state (when PAR = 1200 and 1000 μ mol m⁻² s⁻¹) than under RuBP regeneration-limited state (when PAR = 500 and 300 μ mol m⁻² s⁻¹) (comparing Fig. **6b,d** and Fig. **7b,d**). Again, SIF_{PSII} alone does not appear to have any significant relationship with J_{max25} or V_{cmax25} , regardless of the carboxylation limiting states (Fig. **6a,c** and Fig. **7a,c**). These findings confirm our Hypothesis IV.

Moreover, the regression slopes of J_{max25} (or V_{cmax25}) against $SIF_{\text{PSII}} \times q_L$ are similar between 1200 and 1000 µmol m⁻² s⁻¹ (p = 0.683 for J_{max25} , p = 0.743 for V_{cmax25} , based on two tail t-test), both under the Rubisco-limited state (Fig. **6b,d**). To verify this result with theoretical formula, we checked the composite term of $\frac{1}{f_V(T)} \times \frac{C_l + KCo}{(4C_l + 8\Gamma^*)}$ (eqn 8) under different PAR levels, and found that PAR indeed has minimal impact on the magnitude of this composite term across all temperatures (Fig. **4a**). However, this term is highly sensitive to temperature variations, explaining the divergent J_{max25} (or V_{cmax25}) $\sim SIF_{\text{PSII}} \times q_L$ regression slopes across temperatures (Fig. **3b,d**). Under the RuBP regeneration limitation, there is also no significant difference in the regression slopes of J_{max25} (or V_{cmax25}) against $SIF_{\text{PSII}} \times q_L$ between 500 and 300 µmol m⁻² s⁻¹ (p = 0.725 for J_{max25} , p=0.609 for V_{cmax25}) (Fig. **7b,d**). This can be supported by Fig. **4b**, in which PAR has negligible impact on the

composite term of $\frac{1}{f_V(T)} \times \frac{\theta \cdot \frac{q_L \cdot SIF_{PSII} \cdot (1+k_{DF})}{\sigma \cdot PAR} - \frac{1-\Psi_{PSIImax}}{\Phi_{PSIImax}}}{\frac{q_L \cdot SIF_{PSII} \cdot (1+k_{DF})}{\sigma \cdot PAR} - \frac{1-\Psi_{PSIImax}}{\Phi_{PSIImax}}}$ (eqn 9) across all temperatures. Similar to the composite term in eqn 8, the composite term in eqn 9 is considerably affected by temperatures.

In contrast, the regression slopes of $V_{\rm cmax25}$ (or $J_{\rm max25}$) against $SIF_{\rm PSII} \times q_{\rm L}$ under the Rubisco limitation differ significantly from that under RuBP regeneration limitation when a single PAR for each limitation is considered (*i.e.*, 1200 vs 500, 1200 vs 300, 1000 vs 500, 1000 vs 300). These results suggest that prior information of photosynthetic limitation stage should be considered when observational $SIF_{\rm PSII}$ (or SIF) is employed to infer photosynthetic capacity parameters.

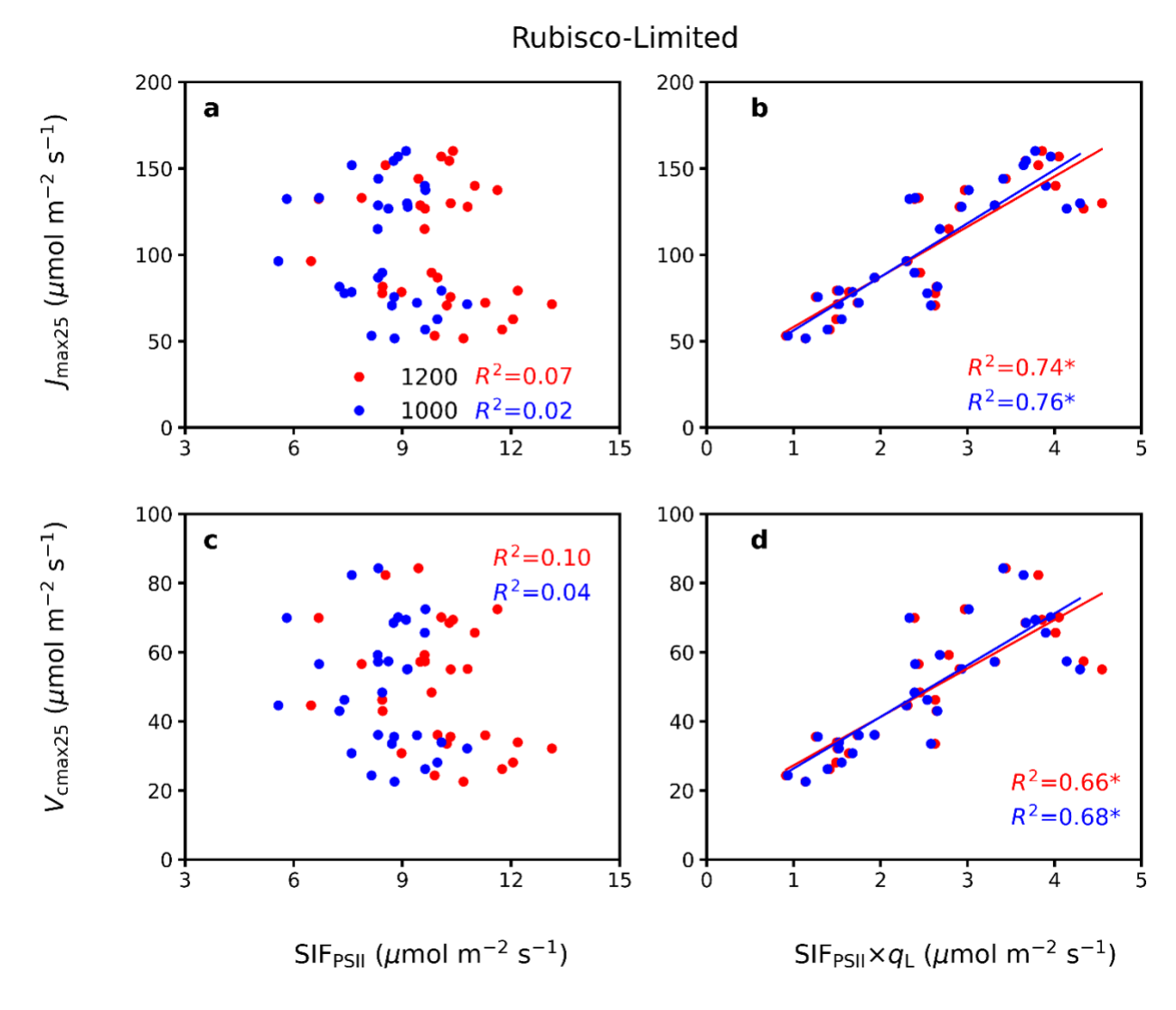


Fig. 6. Similar to Fig.1 but the relationships were analyzed under the Rubisco limitation only. SIF_{PSII} and $SIF_{PSII} \times q_L$ were calculated with ChlF parameters that measured under the PAR of 1200 (red) and 1000 (blue) µmol m⁻² s⁻¹. The linear ordinary least-square regressions were made for each light intensity separately.

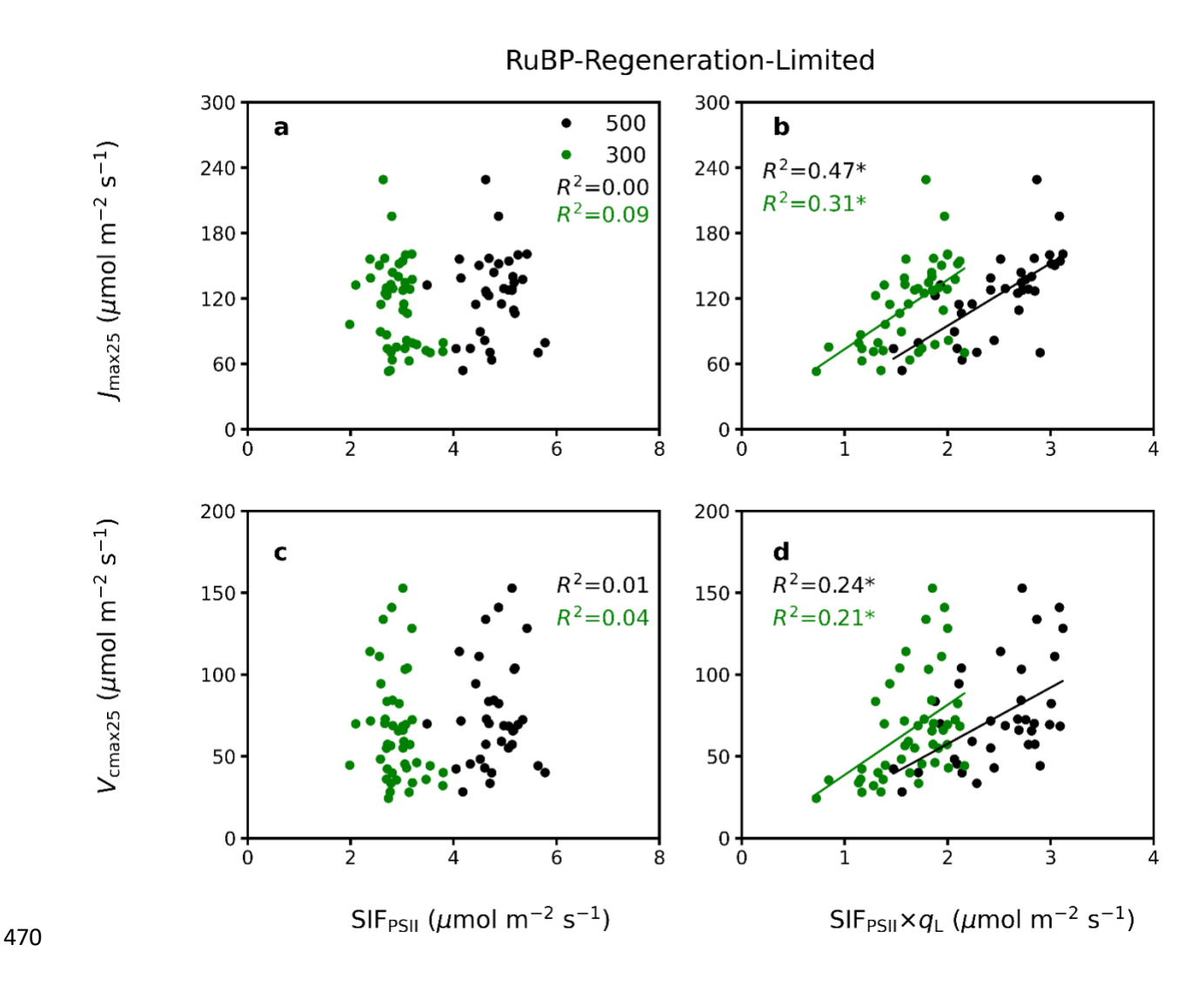


Fig. 7. Similar to Fig. 1 but the relationships were analyzed under the RuBP regeneration limitation only. SIF_{PSII} and $SIF_{PSII} \times q_L$ were calculated with ChlF parameters measured under the PAR of 500 (black) and 300 (green) μ mol m⁻² s⁻¹. The linear ordinary least-square regressions were made for each light intensity separately.

Discussion

475

476

477

478

479

480

481

482

483

484

485

486

487

488

489

490

491

492

493

494

495

496

The product of SIF_{PSII} and q_L has greater capability for inferring photosynthetic capacity

than SIF_{PSII} alone

We observed prominent positive correlation of $SIF_{PSII} \times q_L$ with both J_{max25} and V_{cmax25} across different species under various temperatures and PAR levels, demonstrating that SIF_{PSII}×q_L contains more information on physiological variations related to photosynthetic capacity than SIF_{PSII} alone. This finding can be interpreted mechanistically with eqn 8 and eqn 9, derived by combining MLR-SIF (Gu et al., 2019) and FvCB model (Farguhar et al., 1980) under the assumption of light and carbon reaction balance. q_L reflects the redox state of the electron acceptors in PSII which is highly sensitive to electron transport (Kramer et al., 2004; Baker, 2008). When there is an imbalance between the production of ATP/NADPH at the end of the light reactions and their consumption in the dark reactions which is affected by CO₂ diffusion and photosynthetic capacity, redox reaction rates along the electron transport chain are adjusted instantly (Johnson & Berry, 2021), affecting q_L . Additionally, thylakoid lumen can either acidify or alkalify, depending on the direction of imbalance. Changes in lumen acidity control the energy-dependent component of NPQ and the redox state of the plastoquinone pool (PQ/PQH₂) (a rate-limiting step of electron transport), which is reflected by changes in q_L (Foyer et al., 2012). Thus, the variation of q_L is a result of interactions between the light and carbon reactions, both of which respond to environmental variations (Rochaix, 2011; Roach & Krieger-Liszkay, 2014).

Note that since this study focuses on the functional relationships between SIF_{PSII} (q_L , and $SIF_{PSII} \times q_L$) and photosynthetic capacity parameters instead of their respective absolute values, potential measurement differences induced by instruments (*i.e.*, Li-6800 and GFS-3000) should

not affect our data analysis and conclusions. In addition, this study used modelled SIF_{PSII} (eqn 13), not the directly measured ChlF emission rate to infer photosynthetic capacity parameters. Our rationale is that, in theory, J_a required by MLR-SIF to estimate photosynthesis (and photosynthetic capacity parameters) should be calculated from the ChlF signal from PSII only (denoted as SIF_{PSII}) rather than that contains contributions from both PSII and PSI, which is usually the case for directly observed ChlF emission rate or remotely sensed SIF. Nevertheless, the modeled SIF_{PSII} was thoroughly evaluated with independent ChlF emission spectra elsewhere (Han *et al.*, 2021, under review). Also, we acknowledge that the assumed constants α , β , and k_{DF} in eqn 13 can potentially affect the calculation of SIF_{PSII} , but not the general patterns between photosynthetic capacities and SIF_{PSII} (or $SIF_{PSII} \times q_L$). For facilitating the broad applications of the approach calculating SIF_{PSII} , the values of α , β , and k_{DF} need to be precisely determined in the future.

Factors impacting the relationship between photosynthetic capacity parameters and $SIF_{ m PSII} imes q_{ m L}$

The precise relationships of $SIF_{PSII} \times q_L$ with V_{cmax25} under the Rubisco limitation also depend on C_i according to eqn 8. For broad applications, C_i is often assumed to be a constant ratio of ambient CO_2 concentration C_a (e.g., $C_i/C_a \sim 0.7$ in C_3 species), but it changes with stomatal conductance which is affected directly by VPD and temperatures (Morison & Gifford, 1982). Indeed, the redox state of Q_A , measured by q_L , is a strong predictor of stomatal conductance (Busch, 2014; Glowacka et al., 2018; Kromdijk et al., 2019) and can partly explain the dynamic of stomatal conductance. Thus, modeling stomatal conductance with q_L in the future may eliminate the effects of CO_2 on $SIF_{PSII} \times q_L \sim V_{cmax25}$ relationship. Additionally, to make the method of inferring V_{cmax25} (J_{max25}) with $SIF_{PSII} \times q_L$ applicable beyond the leaf scale, q_L needs to be modelled as a function of

environments (*e.g.*, temperature, PAR, CO₂ levels, and nutrient stress) in future studies, given that it cannot be directly measured at large scales. Under RuBP regeneration limitation, $J_{\text{max}25}$ and $SIF_{\text{PSII}} \times q_{\text{L}}$ might not be linearly correlated, because the variables SIF_{PSII} and q_{L} are still involved in the slope ($\frac{1}{f_V(T)} \times \frac{\theta \cdot \frac{q_L \cdot SIF_{PSII} \cdot (1+k_{DF})}{\sigma \cdot PAR} - \frac{1-\Phi_{PSIImax}}{\Phi_{PSIImax}}}{\frac{1-\Phi_{PSIImax}}{\sigma \cdot PAR}}$ in eqn 9). This further suggests the necessity of modelling q_{L} in the future to explore the environmental factors influencing the relationships between photosynthetic capacity parameters and $SIF_{\text{PSII}} \times q_{\text{L}}$.

519

520

521

522

523

524

525

526

527

528

529

530

531

532

533

534

535

536

537

538

539

540

Besides q_L , eqn 8 and 9 contains other parameters (e.g., k_{DF} , K_{CO} , Γ^* , and $\Phi_{PSIImax}$). These additional parameters are often assumed to be constant in literatures but in reality can vary across plant species and growth environmental conditions (e.g., temperature, water and nutrient stress, and PAR). For example, the actual $k_{\rm DF}$ value is currently unknown. A value of 10 was implied in Pfundel (1998) while Gu et al. (2019) set $k_{\rm DF}$ to 19. The use of these two $k_{\rm DF}$ values would directly cause $V_{\rm cmax25}$ to vary by a factor of two according to eqn 8. Moreover, van der Tol et al. (2014) speculated that k_D (an antenna process) depends on the temperature (even though there is currently no physical mechanism to explain the dependence of k_D on temperatures), which can affect the magnitude of calculated SIF_{PSII} and its response on temperatures. However, the variation of k_D caused by temperature does not impact the general relationship between SIF_{PSII} and V_{cmax25} (or $J_{\text{max}25}$) as k_{DF} remains unchanged under the same temperature and only SIF_{PSII} stratified to a certain abiotic conditions (e.g., same temperature) can be used to infer $V_{\text{cmax}25}$ (demonstrated in Fig. 3). Thus, our conclusion that the product of SIF_{PSII} and q_L has greater capability for inferring photosynthetic capacity than SIF_{PSII} alone still holds true even if temperature has an impact on k_D . In addition, K_{co} and Γ^* are related to the specificity factor of Rubisco, which depend on temperature and the partial pressure of oxygen, and also varies among PFTs (refer to Notes S2). Furthermore,

 Φ_{PSIImax} is relatively conservative (~0.82) across plant species but can decrease under stressed environmental conditions. Given these potential effects of varying environmental conditions, plant species, and growth status (*e.g.*, plant/leaf age, stress) on the parameters involved in our theoretical equations, and consequently the strength of the relationships between SIF_{PSII} , $SIF_{\text{PSII}} \times q_{\text{L}}$, and photosynthetic capacity parameters, more measurements are required in the future to quantitatively examine their relationships across broad biotic and abiotic conditions.

The discrepancies of the relationships between photosynthetic capacity parameters and SIF

(or SIF_{PSII}) among existing studies

Our theoretical and measurement results consistently showed that no general, predictive relationships exist between photosynthetic capacity parameters and *SIF*_{PSII} (due to the regulation of *q*L). This explains the conflicting results reported in previous studies (*e.g.*, Zhang *et al.*, 2014 and Camino *et al.*, 2019 vs Fu *et al.*, 2021 and Koffi *et al.*, 2015). Indeed, from our theoretical formulation (eqn 8-9), it is mechanistically unwarranted to expect simple relationship between photosynthetic capacity parameters and SIF (or *SIF*_{PSII}) across different species and/or environmental conditions even when the measurement settings used to obtain SIF and photosynthetic capacity parameters are exactly the same. It should be noted that the usage of modeled *SIF*_{PSII} (eqn 13) rather than directly measured leaf-level ChIF emission spectra (in absolute radiometric units, *e.g.*, Magney *et al.*, 2019; Meeker *et al.*, 2021) is not the cause of the differences among studies, as a strong correlation between *SIF*_{PSII} and ChIF emission spectra were already confirmed elsewhere (Han *et al.*, under review).

Specifically, our results appear to differ from model simulations (Zhang *et al.*, 2014; Camino *et al.*, 2019), which reported the significant positive relationships between simulated SIF

and V_{cmax25} . The discrepancy might be because our analysis of SIF_{PSII} and photosynthetic capacity parameters relationships were conducted for different plant species, while the existing studies focused on single crop types to infer V_{cmax25} with SIF. To mimic their settings, we pooled our measurements from the same species and performed regression analysis between SIF_{PSII} and photosynthetic capacity parameters (Fig. 8). However, the correlations between SIF_{PSII} and V_{cmax25} (J_{max25}) were still very weak ($R^2 = 0.06$ for V_{cmax25} ; $R^2 = 0.09$ for J_{max25}). A major reason for this weak within-species correlation is that their relationships are affected by any instantaneous or long-term factors that affect photosynthesis. Another possible reason is that, in their studies, SIF was simulated by perturbing V_{cmax25} in SCOPE, a model that was tested only for a limited number of plant types, *i.e.*, crops or temperate young woody plants, grown in greenhouse/chambers/pots, and therefore inevitably suffers from model structure/parameters uncertainties. The derived SIF- V_{cmax25} relationships could thus be inaccurate.

On the other hand, strong negative correlation between $V_{\rm cmax-T}$ and $J_{\rm max-T}$ fitted under measuring air temperatures with $\Phi_{\rm SIF}$ (instead of SIF) was observed among 10 tobacco (*Nicotiana tabacum*) cultivars (Fu *et al.*, 2021). Yet, our study did not find such negative relationship of either $V_{\rm cmax}$ ($J_{\rm max}$) ~ $\Phi_{\rm SIF}$ or $V_{\rm cmax25}$ ($J_{\rm max25}$) ~ $\Phi_{\rm SIF}$ across a wide range of species from different PFTs. Such discrepancy is likely because Fu et al. (2021) confined their analyses to narrowed environmental conditions (*e.g.*, midday only, stratified to different phenological stages) and to a single plant species. In addition, they analyzed the leaf-level $V_{\rm cmax-T}$ and $J_{\rm max-T}$ with $\Phi_{\rm SIF}$ derived from canopy-level measurements of SIF; therefore, the scaling mismatch between leaf and canopy might also have contributed to the observed discrepancies.

Note that this study focuses on the leaf level. Even at the leaf scale the relationship between SIF_{PSII} and photosynthetic capacity parameters is already complex. At the canopy scale, there are additional complexities, *i.e.*, canopy geometry/structure, re-absorption of SIF within the canopy, vertical variations of q_L , that can further affect the strength (and potentially even the sign) of remotely sensed SIF - V_{cmax} (J_{max}) relationships. More measurements at the canopy scale across broad environmental conditions and larger variety of plant species are critically needed in the future.

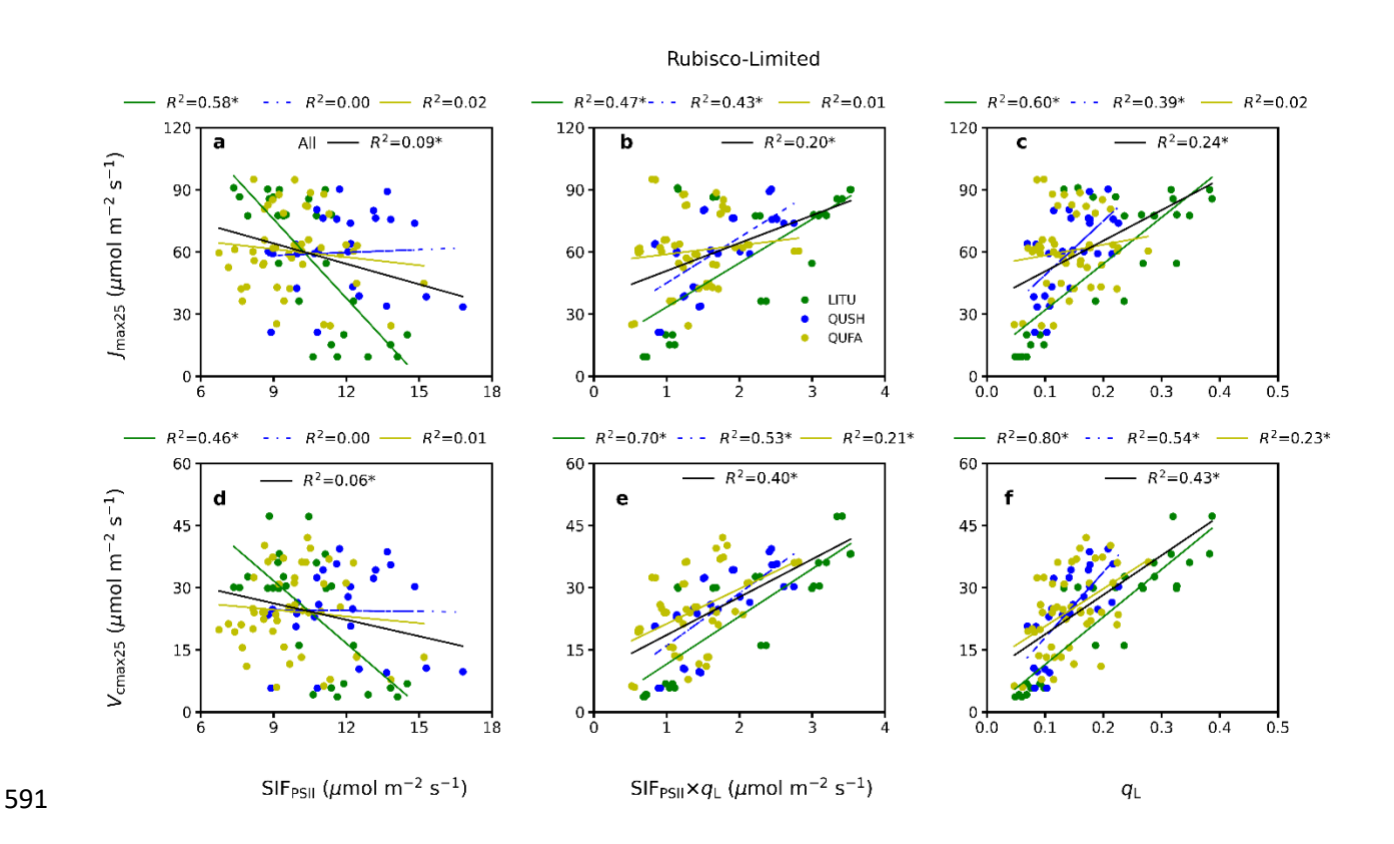


Fig. 8. Similar to Fig. 3, but the data were grouped into different species (LITU: green, QUSH: blue, QUFA: yellow)

Inferring photosynthetic capacity parameters with SIF_{PSII} must consider the photosynthetic limiting stages

595

596

597

598

599

600

601

602

603

604

605

606

607

608

609

610

611

We observed different regression slopes of $V_{\text{cmax}25}$ and $SIF_{\text{PSII}} \times q_{\text{L}}$ between Rubisco and RuBPregeneration limitations, which is theoretically supported by eqn 8 and eqn 9. This suggests that when SIF (or SIF_{PSII}) is used to infer V_{cmax25} , we need a priori information of which photosynthetic limitation the observed SIF (or SIF_{PSII}) is under. The determination of carboxylation limitation state depends on CO₂ level, temperature, PAR, and other environment conditions. To utilize SIF (or SIF_{PSII})× q_L for accurately inferring V_{cmax25} and J_{max25} beyond the leaf level, we need to first determine the carboxylation limitation state with ChlF information itself. Sharkey et al. (2007) reported that ChIF measurements can be used to determine the limiting stages for any data point by analyzing the response of J_a to CO₂ concentration. Similarly, the response of J_a to PAR can be also used to identify the limiting stages. For example, if J_a is increasing with PAR, the data belong to the RuBP-regeneration limitation. If J_a reaches a plateau with PAR, the data are Rubisco-limited. Interestingly, we observed similar patterns between J_a and $SIF_{PSII} \times q_L$ with PAR (Fig. 9), which indicated that the response of $SIF_{PSII} \times q_L$ to environmental factor would be useful to identify the carboxylation limitation states. The consistent trends of J_a and $SIF_{PSII} \times q_L$ can be also explained by the equation of J_a (eqn 1).

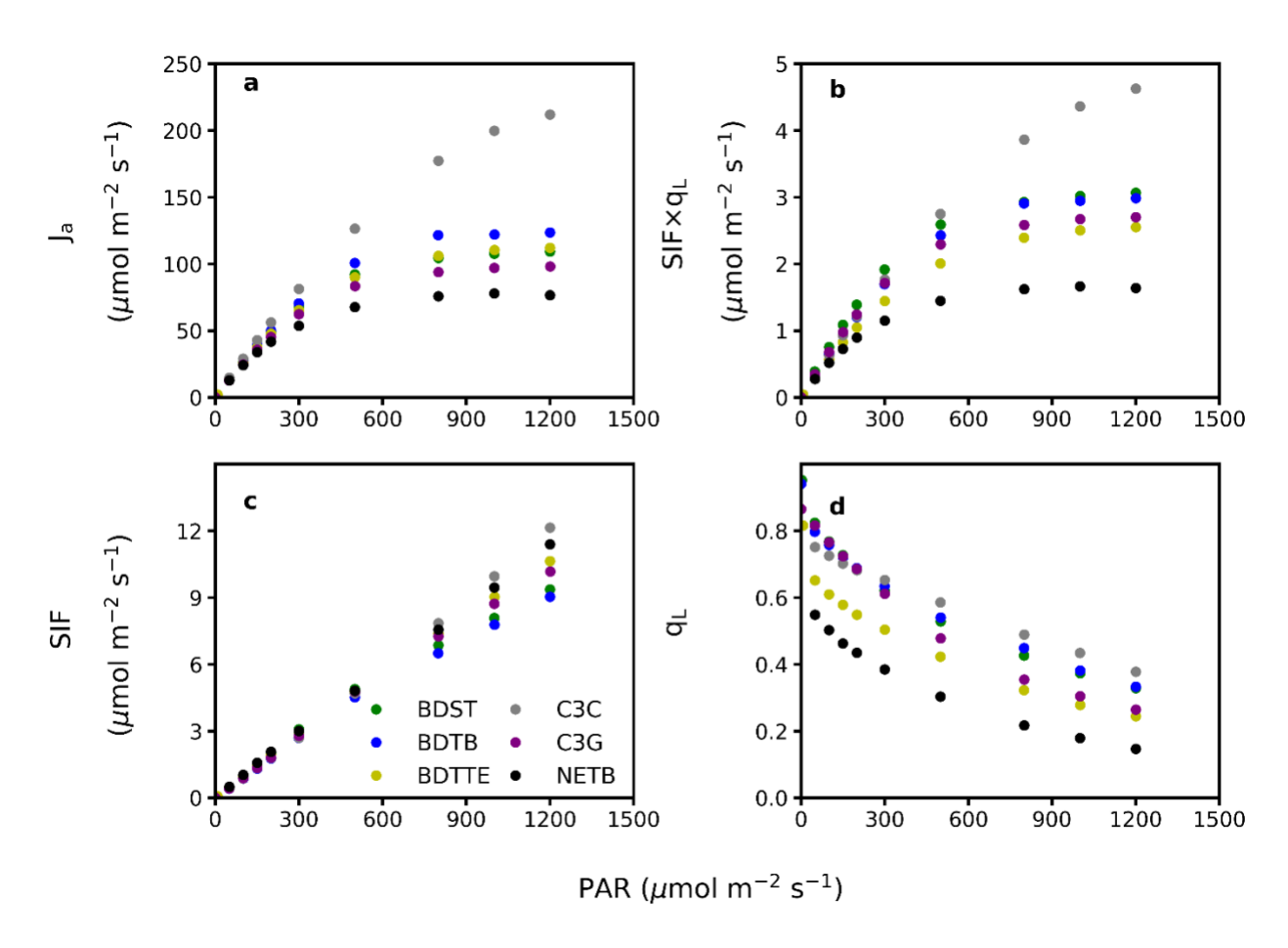


Fig. 9. The response of J_a (a), $SIF_{PSII} \times q_L$ (b), SIF_{PSII} (c), and q_L (d) on PAR at different PFTs. Different colors represent different PFTs. Each scatter represents the mean of all species within the same PFT.

Conclusion

This study revealed that SIF_{PSII} alone is incapable of informing the variations in V_{cmax25} and J_{max25} either within a species or across different species, even when SIF_{PSII} is determined under the same environmental conditions. In contrast, the product of SIF_{PSII} and the fraction of open PSII reaction centers q_L , which indicates the redox state of PSII, is a strong predictor of both V_{cmax25} and J_{max25} . The limitation state of carboxylation must be considered if observed SIF_{PSII} is utilized to infer V_{cmax25} (or J_{max25}) under dynamic environmental conditions. Temperature variations can further complicate the relationships of photosynthetic capacity parameters with $SIF_{PSII} \times q_L$, but such relationships remain relatively stable if considered at the same temperatures. These findings are grounded on the consistency between theoretical reasoning and direct measurements on a diverse number of species and expected to have high rigor and robustness.

Acknowledgments 631 632 This study is supported by NSF Macrosystem Biology (Award 1926488). JH, JW, and YS also acknowledge support from USDA-NIFA Hatch Fund (1014740). ORNL is managed by UT-633 Battelle, LLC, for DOE under contract DE-AC05-00OR22725. 634 **Conflict of Interest** 635 The authors declare that there is no conflict of interest. 636 **Author contributions** 637 JH and YS planned and designed the research. JH performed experiments and analyzed data. JH, 638 639 LG and YS wrote the manuscript. JW performed the statistical analysis. 640 **Data Availability** The data that supports the findings of this study are available in the supplementary material of this 641 article. 642 643 Supplementary data 644 **Notes S1**. The full derivations of the theoretical equations linking photosynthetic capacity 645 parameters with SIF_{PSII} (Eqn 5-6) 646 Notes S2. Validity of the theoretical equations (Eqn 5-6) in directly computing photosynthetic 647 capacity parameters 648 Fig. S1. The relationships between the theoretical $V_{\rm cmax}$ from eqn 5 and that derived from the 649 standard approach across different PFTs (a, for $V_{\rm cmax25}$) and across temperatures for a subset of 650

circle: LITU, triangle: QUSH, square: QUFA) under the Rubisco-limited states.

plant species for which measurements under different temperatures are available (b, for $V_{\rm cmax-T}$,

651

Reference

653

665

- Arrhenius S. 1915. Quantitative Laws in Biological Chemistry, Bell: London.
- Bailey-Serres J, Parker JE, Ainsworth EA, Oldroyd GED, Schroeder J. 2019. Genetic strategies for improving crop yields. *Nature* 575: 109–118.
- 657 **Bernacchi CJ, Singsaas EL, Pimentel C, Portis JR AR, Long SP. 2001.** Improved temperature 658 response functions for models of Rubisco-limited photosynthesis. *Plant Cell and*
- 659 *Environment* **24:** 253–259.

Geophysical Research 116: G02014.

- 660 **Björkman O, Demmig B. 1987.** Photon yield of O₂ evolution and chlorophyll fluorescence characteristics at 77 K among vascular plants of diverse origins. *Planta* **170**: 489–504.
- Bonan GB, Lawrence PJ, Oleson KW, Levis S, Jung M, Reichstein M, Lawrence DM,

 Swenson SC. 2011. Improving canopy processes in the Community Land Model version

 4(CLM4) using global flux fields empirically inferred from FLUXNET data, *Journal of*
- 666 **Busch FA. 2014.** Opinion: the red-light response of stomatal movement is sensed by the redox state of the photosynthetic electron transport chain. *Photosynthetic Research* **119:** 131–140.
- 668 Camino C, Gonzalez-Dugo V, Hernandez P, Zarco-Tejada PJ. 2019. Radiative transfer $V_{\rm cmax}$ 669 estimation from hyperspectral imagery and SIF retrievals to assess photosynthetic
 670 performance in rainfed and irrigated plant phenotyping trials. *Remote Sensing of Environment*671 231: 111186.
- Cooper GM. 2000. The Chloroplast Genome. The Cell: A Molecular Approach (2nd ed.).
 Washington, DC: ASM Press. ISBN 978-0-87893-106-4.

Croft H, Chen JM, Luo X, Bartlett P, Chen B, Staebler RM. 2017. Leaf chlorophyll content as 674 a proxy for leaf photosynthetic capacity. Global Change Biology 23: 3513–3524. 675 Demmig-Adams B, Garab G, Adams III W, Govindjee, Eds. 2014. "Non-Photochemical 676 Quenching and Energy Dissipation" in Plants, Algae and Cyanobacteria (Springer, 677 Dordrecht). 678 **Detto M, Xu X. 2020.** Optimal leaf life strategies determine $V_{\rm cmax}$ dynamic during ontogeny. New 679 680 Phytologist 228: 361–375. 681 Farquhar GD, von Caemmerer S, Berry JA. 1980. A biochemical model of photosynthetic CO₂ assimilation in leaves of C3 species. *Planta* **149**: 78–90. 682 Field C, Mooney HA. 1986. The photosynthesis-nitrogen relationship in wild plants. In: Givnish 683 T, eds. On the Economy of Plant Form and Function. Cambridge University Press, 25–55. 684 Foyer CH, Neukermans J, Queval G, Noctor G, Harbinson J. 2012. Photosynthetic control of 685 686 electron transport and the regulation of gene expression. Journal of Experimental Botany 63: 1637–1661. 687 688 Frankenberg C, Fisher JB, Worden J. 2011. New global observations of the terrestrial carbon cycle from GOSAT: Patterns of plant fluorescence with gross primary productivity. 689 Geophysical Research Letters. 38: L17706. 690 Fu P, Meacham-Hensold K, Siebers MH, Bernacchi CJ. 2021. The inverse relationship between 691 692 solar-induced fluorescence yield and photosynthetic capacity: benefits for field phenotyping. Journal of Experimental Botany 72: 1295–1306. 693

- Fu P, Meacham-Hensold K, Guan K, Bernacchi CJ. 2019. Hyperspectral leaf reflectance as proxy for photosynthetic capacities: an ensemble approach based on multiple machine learning algorithms. *Frontiers in Plant Science* 10: 730.
- Genty B, Briantais J-M, Baker NR. 1989. The relationship between the quantum yield of
 photosynthetic electron transport and quenching of chlorophyll fluorescence. *Biochimica et Biophysica Acta* 990: 87–92.
- Glowacka K, Kromdijk J, Kucera K, Xie J, Cavanagh AP, Leonelli L, Leakey ADB, Ort DR,
 Niyogi KK, Long SP. 2018. Photosystem II Subunit S overexpression increases the
 efficiency of water use in a field-grown crop. *Nature Communication* 9: 868.
- Gu LH, Han JM, Wood JW, Sun Y. 2019. Sun-induced Chl fluorescence and its importance for
 biophysical modeling of photosynthesis based on light reactions. *New Phytologist* 223: 1179–
 1191.
- Gu LH, Pallardy SG, Tu K, Law BE, Wullschleger SD. 2010. Reliable estimation of biochemical parameters from C3 leaf photosynthesis-intercellular carbon dioxide response curves. *Plant Cell Environment* 33: 1852–1874.
- Guanter L, Frankenberg C, Dudhia A, Lewis PE, Gómez-Dans J, Kuze A, Suto H, Grainger
 RG. 2012. Retrieval and global assessment of terrestrial chlorophyll fluorescence from
 GOSAT space measurements. Remote Sensing of Environment 121: 236–251.
- Johnson F, Eyring H, Williams R. 1942. The nature of enzyme inhibitions in bacterial luminescence: sulphanilamide, urethane, temperature, pressure. *Journal of Cell Comparative Physiology* 20: 247–268.

- Johnson JE, Berry JA. 2021. The role of Cytochrome b₆f in the control of steady-state
- photosynthesis: a conceptual and quantitative model. *Photosynthesis Research* **148:** 101–136.
- Joiner J, Guanter L, Lindstrot R, Voigt M, Vasilkov AP, Middleton EM, Huemmrich KF,
- Yoshida Y, Frankenberg C. 2013. Global monitoring of terrestrial chlorophyll fluorescence
- from moderate spectral resolution near-infrared satellite measurements: Methodology,
- simulations, and application to GOME-2. Atmospheric Measurement Techniques 6: 2803–
- 721 2823.
- Joliot P, Johnson GN. 2011. Regulation of cyclic and linear electron flow in higher plants. *Proc*
- 723 *Natl Acad Sci USA* **108:** 13317–13322.
- Kattge J, Bönisch G, Díaz S, Lavorel S, Prentice IC, Leadley P, Tautenhahn S, Werner GDA,
- 725 Aakala T, Abedi M et al. 2020. TRY plant trait database enhanced coverage and open
- access. Global Change Biology 26: 119–188.
- 727 Koffi EN, Rayner PJ, Norton AJ, Frankenberg C, Scholze M. 2015. Investigating the
- usefulness of satellite-derived fluorescence data in inferring gross primary productivity
- within the carbon cycle data assimilation system. *Biogeosciences* **12:** 4067–4084.
- 730 Kramer DM, Evans JR. 2011. The importance of energy balance in improving photosynthetic
- productivity. *Plant Physiology* **155:** 70–78.
- Kramer DM, Johnson G, Kiirats O, Edwards GE. 2004. New fluorescence parameters for the
- determination of Q_A redox state and excitation energy fluxes. *Photosynthesis Research* **79**:
- 734 209–218.

Kromdijk J, Glowacka K, Long SP. 2019. Predicting light-induced stomatal movements based 735 on the redox state of plastoquinone: theory and validation. *Photosynthesis Research* 141: 83– 736 97. 737 738 Long SP, Postl WF, Bolharnordenkampf HR. 1993. Quantum yields for uptake of carbon dioxide in C3 vascular plants of contrasting habitats and taxonomic groupings. Planta 189: 739 740 226-234. Magney TS, Frankenberg C, Köhler P, North G, Davis TS, Dold C, Dutta D, Fisher JB, 741 Grossmann K, Harrington A et al. 2019. Disentangling changes in the spectral shape of 742 chlorophyll fluorescence: Implications for remote sensing of photosynthesis. Journal of 743 *Geophysical Research: Biogeosciences* **124:** 1491–1507. 744 Meacham-Hensold K, Montes CM, Wu J, Guan K, Fu P, Ainsworth EA, Pederson T, Moore 745 CE, Brown KL, Raines C, Bernacchi CJ. 2019. High-throughput field phenotyping using 746 hyperspectral reflectance and partial least squares regression (PLSR) reveals genetic 747 modifications to photosynthetic capacity. Remote Sensing of Environment 231: 111176. 748 Medlyn BE, Dreyer E, Ellsworth D, Forstreuter M, Harley PC, Kirschbaum MUF, le Roux 749 X, Montpied P, Strassemeyer J, Walcroft A, Wang K, Loustau D. 2002. Temperature 750 response of parameters of a biochemically based model of photosynthesis. II. A review of 751 experimental data. Plant, Cell and Environment 25: 1167–1179. 752 753 Meeker EW, Magney TS, Bambach N, Momayyezi M, McElrone AJ. 2021. Modification of a gas exchange system to measure active and passive chlorophyll fluorescence simultaneously 754 under field conditions. AoB Plants doi:10.1093/aobpla/plaa066. 755 Mohammed GH, Colombo R, Middleton EM. 2019. Remote sensing of solar-induced 756

757

chlorophyll fluorescence (SIF) in vegetation: 50 years of progress. Remote Sensing of

- 758 *Environment* **231:** 111177.
- 759 Morison JIL, Gifford RM. 1982. Stomatal Sensitivity to Carbon Dioxide and Humidity. A
- comparison of two C3 and two C4 grass species. *Plant Physiology* **71:** 789–796.
- Oxborough K, Baker NR. 1997. Resolving chlorophyll a fluorescence images of photosynthetic
- efficiency into photochemical and non-photochemical components-calculation of qP and
- 763 $F_{\rm v}$ '/ $F_{\rm m}$ ' without measuring $F_{\rm o}$ '. *Photosynthsis Research* **54**:135–142.
- Papageorgiou GC, Govindjee G. 2004. Chlorophyll Fluorescence: A Signature of Photosynthesis.
- 765 Springer, Dordrecht.
- Porcar-Castell A, Tyystjärvi E, Atherton J, van der Tol C, Flexas J, Pfündel EE, Moreno J,
- Frankenberg C, Berry JA. 2014. Linking chlorophyll a fluorescence to photosynthesis for
- remote sensing applications: mechanisms and challenges. *Journal of Experimental Botany* **65:**
- 769 4065–4095.
- Pospisil P, Skotnica J, Naus J. 1998. Low and high temperature dependence of minimum F_0 and
- maximum $F_{\rm M}$ chlorophyll fluorescence in vivo. *Biochimica et Biophysica Acta* **1363:** 95–99.
- 772 Roach T, Krieger-Liszkay A. 2014. Regulation of photosynthetic electron transport and
- photoinhibition. *Current Protein and Peptide Science* **15:** 351–362.
- 774 **Rochaix JD. 2011.** Regulation of photosynthetic electron transport. *Biochimica et Biophysica Acta*
- *Bioenergetics* **1807:** 375–383.
- Rogers A, Medlyn BE, Dukes JS, Bonan G, von Caemmerer S, Dietze MC, Kattge J, Leakey
- ADB, Mercado LM, Niinemets Ü et al. 2017. A roadmap for improving the representation
- of photosynthesis in Earth system models. *New Phytologist* **213**: 22–42.

- Schaefer K, Schwalm CR, Williams C, Arain MA, Barr A, Chen JM, Davis KJ, Dimitrov D,
- 780 Hilton TW, Hollinger DY et al. 2012. A model-data comparison of gross primary
- productivity: Results from the North American Carbon Program site synthesis. *Journal of*
- *Geophysical Research: Biogeosciences* **117:** G03010.
- 783 Schreiber U. 2004. Pulse-Amplitude-Modulation (PAM) Fluorometry and Saturation Pulse
- Method: An Overview. In: Papageorgiou G.C., Govindjee (eds) Chlorophyll a Fluorescence.
- Advances in Photosynthesis and Respiration, Springer, Dordrecht, **19:** 279–319.
- 786 Serbin SP, Singh A, Desai AR, Dubois SG, Jablonski AD, Kingdon CC, Kruger EL,
- **Townsend PA. 2015.** Remotely estimating photosynthetic capacity, and its response to
- temperature, in vegetation canopies using imaging spectroscopy. Remote Sensing of
- 789 *Environment* **167:** 78–87.
- 790 Sharkey TD, Bernacchi CJ, Farquhar GD, Singsaas EL. 2007. Fitting photosynthetic carbon
- dioxide response curves for C3 leaves. *Plant, Cell, and Environment* **30:** 1035–1040.
- 792 Sharkey TD. 1985. O2-insensitive photosynthesis in C3 plants: its occurrence and a possible
- 793 explanation. *Plant Physiology* **78:** 71–75.
- 794 Simkin AJ, López-Calcagno PE, Raines CA. 2019. Feeding the world: improving
- 795 photosynthetic efficiency for sustainable crop production. *Journal of Experimental Botany*
- **70:** 1119–1140.
- 797 Simkin AJ, McAusland L, Headland LR, Lawson T, Raines CA. 2015. Multigene manipulation
- of photosynthetic carbon assimilation increases CO2 fixation and biomass yield in tobacco.
- *Journal of Experimental Botany* **66:** 4075–4090.

- 800 South PF, Cavanagh AP, Liu HW, Ort DR. 2019. Synthetic glycolate metabolism pathways stimulate crop growth and productivity in the field. Science 363(6422): eaat9077. 801 802 Stinziano JR, Roback C, Gamble D, Murphy B, Hudson P, Muir CD. 2020. Photosynthesis: 803 tools for plant ecophysiology & modeling. R package version 2.0.1. Tesa M, Thomson S, Gakamsky A. 2018. Temperature-dependent quantum yield of fluorescence 804 805 from plant leaves. Application notes in Edinburgh instruments. AN P41. Vilfan N, van der Tol C, Verhoef W. 2019. Estimating photosynthetic capacity from leaf 806 reflectance and Chl fluorescence by coupling radiative transfer to a model for photosynthesis. 807 808 *New Phytologist* **223:** 487–500. van der Tol C, Berry JA, Campbell PKE. 2014. Models of fluorescence and photosynthesis for 809 810 interpreting measurements of solar-induced chlorophyll fluorescence. Journal of Geophysical Research: Biogeosciences 119: 2312–2327. 811 van der Tol C, Verhoef W, Timmermans J, Verhoef A, Su Z. 2009. An integrated model of 812 soil-canopy spectral radiances, photosynthesis, fluorescence, temperature and energy 813 814 balance. *Biogeosciences* **6:** 3109–3129. von Caemmerer S, Farquhar GD. 1981. Some relationships between the biochemistry of 815 photosynthesis and the gas exchange of leaves. *Planta* **153**: 376–387. 816 817 von Caemmerer S. 2000. Biochemical Models of Leaf Photosynthesis. Techniques in Plant
 - Walker AP, Beckerman AP, Gu L, Kattge J, Cernusak LA, Domingues TF, Scales JC,

Science, No. 2. CSIRO Publishing, Collingwood.

818

- Wohlfahrt G, Wullschleger SD, Woodward FI. 2014. The relationship of leaf photosynthetic traits $V_{\rm cmax}$ and $J_{\rm max}$ to leaf nitrogen, leaf phosphorus, and specific leaf area: a meta-analysis and modeling study. *Ecology and Evolution* 4: 3218–3235.
- Wright IJ, Reich PB, Westoby M, Ackerly DD, Baruch Z, Bongers F, Cavender-Bares J,

 Chapin FS, Cornelissen JHC, Diemer M et al. 2004. The world-wide leaf economics

 spectrum. *Nature* 428: 821–827.
- Wullschleger SD. 1993. Biochemical limitations to carbon assimilation in C3 plants a retrospective analysis of the A/Ci curves from 109 species. *Journal of Experimental Botany* 44: 907–920.
- Xu L, and Baldocchi DD. 2003. Seasonal trend of photosynthetic parameters and stomatal conductance of blue oak (Quercus douglasii) under prolonged summerdrought and high temperature. *Tree Physiology* 23: 865–877.
- Yendrek CR, Tomaz T, Montes CM, Cao Y, Morse AM, Brown PJ, McIntyre LM, Leakey

 ADB, Ainsworth EA. 2017. High-Throughput Phenotyping of Maize Leaf Physiological and

 Biochemical Traits Using Hyperspectral Reflectance. *Plant Physiology* 173: 614–626.
- Yin X, Busch FA, Struik PC, Sharkey TD. 2021. Evolution of a biochemical model of steadystate photosynthesis. *Plant, cell and environment*. https://doi.org/10.1111/pce.14070.
- **Yoshikawa M. 2013.** Handbook of Biologically Active Peptides (Second Edition). 1570–1576.

838

839

840

Zhang Y, Guanter L, Joiner J, Song L, Guan K. 2018. Spatially-explicit monitoring of crop photosynthetic capacity through the use of spacebased chlorophyll fluorescence data. *Remote Sensing of Environment* **210:** 362–374.

Zhang YG, Guanter L., Berry JA, Joiner J., van der T, Huete A, Gitelson A, Voigt M, Kohler
 P. 2014. Estimation of vegetation photosynthetic capacity from space-based measurements
 of chlorophyll fluorescence for terrestrial biosphere models. Global Change Biology 20:
 3727–3742.

846	Inference of photosynthetic capacity parameters from Chlorophyll a Fluorescence is
847	affected by the redox state of PSII reaction centers
848	Running title: The role of q_L in inferring V_{cmax} using SIF_{PSII}
849	Jimei Han ¹ *, Lianhong Gu ² , Jiaming Wen ¹ , Ying Sun ¹ *
850 851	¹ School of Integrative Plant Science, Soil and Crop Science Section, Cornell University, Ithaca, NY, USA
852	² Environmental Sciences Division and Climate Change Science Institute, Oak Ridge National
853	Laboratory, Oak Ridge, Tennessee, USA
854	*Corresponding to: jh2757@cornell.edu (J. Han), ys776@cornell.edu (Y. Sun)
855	

- Notes S1. The full derivations of the theoretical equations linking photosynthetic capacity
- 857 parameters with SIF_{PSII} (Eqn 5-6)
- By equating the light reaction-based (MLR-SIF, eqn 1) and carbon reaction-based J_a (FvCB, eqn
- 859 2-3), we can derive explicit relationships between SIF_{PSII} and $V_{\rm cmax}$ (and $J_{\rm max}$). Specifically, under
- the Rubisco-limited state, set $A_g = A_c$; then combining eqn 2 and 3b leads to:

861
$$\frac{V_{cmax} \cdot (C_i - \Gamma^*)}{C_i + Kco} = \frac{(C_i - \Gamma^*)}{4C_i + 8\Gamma^*} \times J_a.$$
 (eqn 4 in the main text)

862 Inserting eqn 1 to eqn 4 results in:

863
$$\frac{V_{cmax} \cdot (C_i - \Gamma^*)}{C_i + Kco} = \frac{(C_i - \Gamma^*)}{4C_i + 8\Gamma^*} \times \frac{\Phi_{PSIImax} \cdot (1 + k_{DF})}{1 - \Phi_{PSIImax}} \times q_L \times SIF_{PSII}.$$
 (S1)

864 Thus,

865
$$V_{cmax} = \frac{C_i + Kco}{(4C_i + 8\Gamma^*)} \times \frac{\Phi_{PSIImax}}{1 - \Phi_{PSIImax}} \times (1 + k_{DF}) \times q_L \times SIF_{PSII}.$$
 (eqn 5 in the main text)

Within the FvCB framework, the potential electron transport rate J_p is empirically calculated by:

867
$$J_p = \frac{\sigma \cdot PAR + J_{max} - \sqrt{(\sigma \cdot PAR + J_{max})^2 - 4\theta \cdot \sigma \cdot PAR \cdot J_{max}}}{2\theta}.$$
 (eqn 3d in the main text)

868 Eqn S3d is a root of the following quadratic equation:

869
$$\theta \cdot J_p^2 - (\sigma \cdot PAR + J_{max})J_p + J_{max} \cdot \sigma \cdot PAR = 0.$$
 (S2)

870 Or equivalently,

871
$$J_p = \frac{J_{max} - J_p}{J_{max} - \theta \cdot J_p} \bullet \sigma \bullet PAR.$$
 (S3)

872 Eqn S3 shows that the FvCB model for potential electron transport is a recursive model.

Under the RuBP regeneration limited state, the potential electron transport rate becomes the actual

rate, *i.e.*, $J_p = J_a$. Solve eqn S3 for J_{max} :

875
$$J_{max} = \frac{\theta \cdot J_a - \sigma \cdot PAR}{J_a - \sigma \cdot PAR} J_a. \tag{S4}$$

876 Insert eqn 3d into S4:

877
$$J_{max} = \frac{\theta \cdot \frac{q_L \cdot SIF_{PSII} \cdot (1+k_{DF})}{\sigma \cdot PAR} - \frac{1 - \Phi_{PSIImax}}{\Phi_{PSIImax}}}{\frac{\Phi_{PSIImax}}{\sigma \cdot PAR}} \times \frac{\Phi_{PSIImax}}{1 - \Phi_{PSIImax}} \times (1+k_{DF}) \times q_L \times SIF_{PSII}$$
(eqn 6 in

878 the main text)

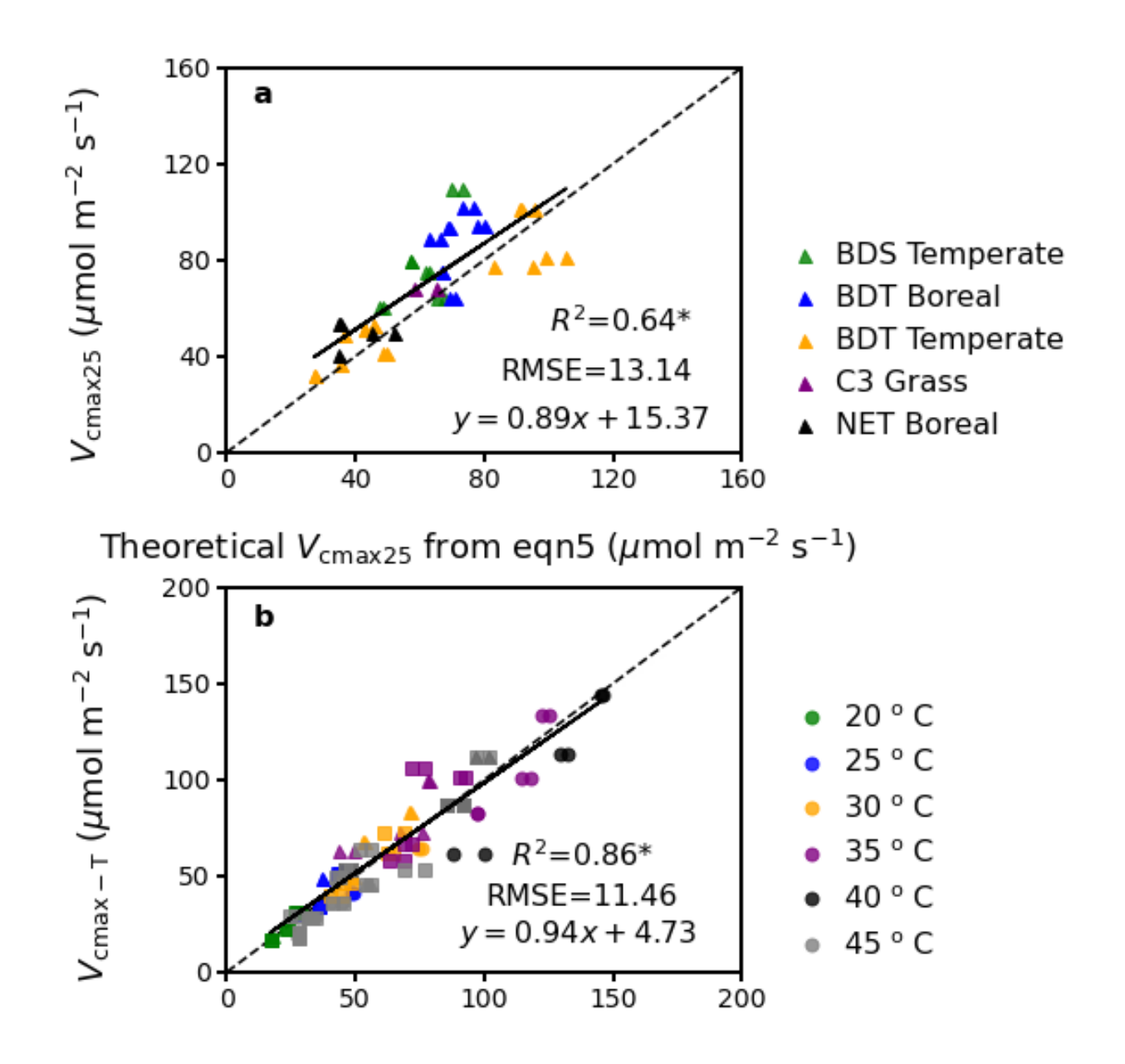
Notes S2. Validity of the theoretical equations (Eqn 5-6) in directly computing photosynthetic

881 capacity parameters

To demonstrate the validity of our theoretical formulations in directly deriving photosynthetic capacity parameters, we compared $V_{\rm cmax}$ computed from eqn 5 (using $V_{\rm cmax}$ only here as an example for illustrative purpose) by assuming the unknown parameters as constants, against that determined from the standard approach, *i.e.*, fitting CO₂ and light response curves based upon the FvCB model using the *photosynthesis* R package (Stinziano *et al.*, 2020) (details in the main text). Specifically, to compute $V_{\rm cmax}$ with eqn 5, we assumed $k_{\rm DF}$ to be 10 for all the PFT species under different temperatures (20, 25, 30, 35, 40, and 45 °C). Γ^* and $K_{\rm co}$ were assumed to be constant at 42.75 µmol mol⁻¹ and 435.44 µmol mol⁻¹, respectively at 25 °C (Bernacchi *et al.*, 2001) and constant across plant species. The temperature response function from Bernacchi *et al.* (2001) was adopted to calibrate Γ^* and $K_{\rm co}$ at other temperatures. Then, the derived $q_{\rm L}$, $SIF_{\rm PSII}$, and $\Phi_{\rm PSIImax}$ using PAM parameters and directly measured $C_{\rm i}$ at saturating light (1000 and 1200 µmol m⁻² s⁻¹) and ambient CO₂ conditions (400 µmol mol⁻¹) under Rubisco-limited states were used to compute $V_{\rm cmax}$ with eqn 5 under different temperatures across different plant species.

We observed that the $V_{\rm cmax}$ theoretically derived from eqn 5 was strongly correlated with that determined from the standard approach (Fig. S1). Specifically, for $V_{\rm cmax25}$, their R² is 0.64

with a regression slope of 0.89 (p<0.05) across PFTs (Fig. S1); for $V_{\rm cmax-T}$ their R² is 0.86 with a regression slope of 0.94 (p<0.05) across temperatures for a subset of species (for which measurements under different temperatures are available, *i.e.*, LITU, QUSH, and QUFA). This result demonstrates the validity of our theoretical formulation that computes photosynthetic parameters with $SIF_{\rm PSII}$. Notably, the regression slope in Fig. S1a, to some degree, deviates from the 1:1 line, which is likely a consequence of the assumed constant values for Γ^* and $K_{\rm co}$ across PFTs. This indicates that the use of assumed constants for unknown parameters can contribute to the uncertainty of our theoretical formulation for practical applications. In addition, mesophyll conductance was assumed to be infinite for $V_{\rm cmax}$ derived from both approaches here, which could result in the underestimation of $V_{\rm cmax}$ and $J_{\rm max}$ (Sun *et al.*, 2014). Therefore, broad applications of our theoretical formulations would require a coupling with mesophyll conductance model in the future.



Theoretical V_{cmax-T} from eqn5 (μ mol m⁻² s⁻¹)

Fig. S1. The relationships between the theoretical $V_{\rm cmax}$ from eqn 5 and that derived from the standard approach across different PFTs (a, for $V_{\rm cmax25}$) and across temperatures for a subset of plant species for which measurements under different temperatures are available (b, for $V_{\rm cmax-T}$, circle: LITU, triangle: QUSH, square: QUFA) under the Rubisco-limited states. The black lines are linear ordinary least-square regression with all data pooled together. * denotes statistically significant at the level of 0.05. Each scatter represents one single leaf replicate. The

theoretical V_{cmax} from eqn 5 was calculated under the PAR of 1200 and 1000 μmol m⁻² s⁻¹ and ambient CO₂ conditions (400 μmol mol⁻¹) at 25 °C for (a) and different temperatures (20, 25, 30, 35, 40, 45 °C) for (b). The data size for each species or temperature depends on how many data samples were Rubisco-limited.